Alma Mater Studiorum - University of Bologna

SCHOOL OF ENGINEERING AND ARCHITECTURE

DEPARTMENT OF INDUSTRIAL ENGINEERING

SECOND CYCLE DEGREE IN ENERGY ENGINEERING

MASTER'S THESIS

in

Sustainable Technologies for Energy Resources

MODELLING OF COMBUSTION GENERATED DURING THE RUPTURE OF HYDROGEN TANKS

Submitted by:
Gabriele Tincani

Supervisor:
Prof. Ernesto Salzano

Co-Supervisors:
Prof. Federico Ustolin
Eng. Leonardo Giannini
Prof. Nicola Paltrinieri

Academic Year 2021/2022
Session III

Abstract

Hydrogen is considered one of the possible solutions to reduce greenhouse gas emissions. However, there are production, storage, and safety issues to be solved before it might start to be widely used worldwide. In this thesis, the fireballs generated after the catastrophic rupture of hydrogen tanks are studied. In particular, the fireball thermal hazard is evaluated by means of experimental data collected during the SH2IFT project. Also, the models generally used to predict the fireball dimension and duration are analyzed and compared with empirical data from the literature. Finally, some new models that better describe the experimental data are proposed.

Contents

1 Introduction **1**

2 State of the art of loss of containment of hydrogen storage **3**

2.1 Hydrogen storage . . . 3

2.1.1 Physical storage . . . 3

2.1.2 Other storage systems . . . 8

2.2 Loss of containment in hydrogen equipment . . . 9

2.2.1 Hydrogen Damages . . . 9

2.2.2 Thermal and mechanical stress . . . 12

2.3 Loss of containment consequences . . . 13

2.3.1 Boiling Liquid Expanding Vapor Explosion . . . 13

2.3.2 Pressure Vessel Burst . . . 18

2.3.3 Continuous releases . . . 19

2.4 Fireball analysis . . . 20

2.4.1 Fireball theory . . . 20

2.4.2 Fireball models . . . 21

3 Case studies **27**

3.1 BLEVE tests . . . 27

3.1.1 BMW test series . . . 28

3.1.2 SH2IFT project . . . 29

3.2 Compressed hydrogen tests . . . 30

3.2.1 Zalosh tests . . . 30

3.2.2 Tamura tests . . . 31

3.2.3 Shen test . . . 31

3.3 NASA tests . . . 32

4 Materials and methods **35**

4.1 Fireball models . . . 35

4.1.1 Heat radiation . . . 36

4.1.2 Thermal dose and thermal hazard . . . 37

4.1.3 Fireball dimension and duration 38

5 Results and discussion **43**
5.1 SH2IFT project 43
5.1.1 Fireball surface emissive power 43
5.1.2 Heat radiation 46
5.1.3 Thermal dose and safety distances 48
5.2 PVBs and BLEVEs prediction models 52
5.2.1 Fireball diameter 53
5.2.2 Fireball duration 57
5.3 NASA tests 60
5.3.1 Fireball dimension and duration 60

6 Conclusions **63**

Appendices **64**

A Heat Capacities at Constant Pressure of Chemical Compounds **65**

B Thermal effects with steady view factor **67**

C Thermal effects with dynamic view factor **71**

Bibliography **82**

1 Introduction

Since the end of the 20th century, the need to reduce greenhouse gas (GHG) emissions to mitigate climate change has led increasingly more countries and industries to rethink their way to produce and consume energy. Some international agreements, like the Kyoto Protocol in 1997 [1] and the Paris Agreement in 2015 [2], are evidence of this effort.

Even if nowadays almost 80% of the energy production is still linked to fossil fuels consumption [3], low-carbon energy sources, like renewables and nuclear, are gaining increasing interest worldwide. In particular, wind and solar photovoltaic are experiencing great momentum, with the provisions of reaching together 70% of the global electricity generation in 2050 [3]. However, these energy sources are intermittent and unpredictable, since they depend on the weather conditions, and some challenges are yet to be overcome before they will be able to completely replace fossil fuels.

One of the main challenges is related to the need for great storage systems, in order to decouple electricity production from its consumption, reducing also the curtailment in the renewables power plants, that is the intentional reduction in the energy output below the maximum that can be produced because of low energy demand by the power grid. One possible solution might be found in hydrogen (H_2), as shows the increasing interest that this energy carrier is getting worldwide, as reported by the International Energy Agency in its report "The Future of Hydrogen"[4].

Hydrogen is a small molecule, that on Earth is often found bounded by other elements to form chemical compounds. For this reason, it is usually not considered an energy source, but an energy carrier. Indeed, it can be produced from fossil fuels or from water through electrolysis, stored, and used later to generate electricity. Furthermore, it might be also utilized in the hard-to-abate sectors, where electrification is not feasible.

However, some issues have to be solved before hydrogen might start to be widely used worldwide. Both hydrogen production and storage require high technical or expensive solutions to be overcome, related to energy consumption and to the H_2 low density. In addition, there are safety issues related to the use of hydrogen. Indeed, it is a very reactive molecule, with a low minimum ignition energy (0.017mJ [5]) and a wide range of flammability (concentrations of 4-75%vol in air [6]). Also, hydrogen might deteriorate the materials it comes into contact with if they are not selected prop-

erly, potentially leading to a critical inhibition of several mechanical properties of the implemented materials [7].

In particular, this thesis focuses on the fireballs generated from the catastrophic rupture of hydrogen tanks. The fireball thermal hazard is studied by taking into account the experimental data related to the heat radiation, collected during the SH2IFT project [8]. SH2IFT is the abbreviation of *Safe Hydrogen Fuel Handling and Use for Efficient Implementation*, which was a project, that lasted from 2018 to 2022, with the aim of increasing the competence and knowledge related to the safety of hydrogen technologies [9].

Then, the models present in the literature used to predict the fireball dimension and duration are analyzed, comparing them with the empirical data coming from the SH2IFT project and other tests that investigated the Boiling Liquid Expanding Vapor Explosion (BLEVE) and Pressure Vessel Burst (PVB) accidents consequences. Finally, some new models that better describe the experimental data are proposed as an overall result, along with a discussion on the limitation of the adopted approach.

2 State of the art of loss of containment of hydrogen storage

In this chapter, an overview of the different types of hydrogen storage is presented, giving more focus to compressed hydrogen tanks and liquefied hydrogen vessels. Then, hazards related to the failure of hydrogen tanks are presented and the major consequences are analyzed. In the last part of the chapter, the different stages of fireball development are discussed and the models used to characterize it are presented.

2.1 Hydrogen storage

Hydrogen is the most common element in nature, but on Earth, it can be mostly found bonded with other atoms forming chemical compounds. In order to use it as an energy carrier, it has to be produced and stored. At normal temperature and pressure (NTP) conditions (293K, 101.325kPa), hydrogen has a very low density (0.083732kg/m^3 [10]) compared to the other fuels. This leads to larger storage volumes and high investment costs. For this reason, different storage methods have been developed in the last decades. Storage systems can be divided into three different categories: *(i)* hydrogen can be stored as compressed gas or as a liquid; *(ii)* it can be adsorbed into materials, thanks to the physical van der Waals bonds; *(iii)* it can be stored as hydrides, through chemical bonds [11]. This classification is summarized in Figure 2.1.

2.1.1 Physical storage

The most common way of storing hydrogen is through physical storage. Using structural vessels or underground cavities, the density of the hydrogen can be changed thanks to the variation in pressure and temperature. In particular, the increase in pressure and the reduction in temperature lead to density growth, as Figure 2.2 shows.

Four different approaches for hydrogen storage are usually used:

- Compressed hydrogen tanks operating at high pressures, up to 70MPa, and ambient temperature;
- Cold-compressed hydrogen vessels operating at high pressure (around 50MPa), but lower temperatures (between 150K and 273K) [12];
- Cryo-compressed hydrogen tanks operating at pressure under 35MPa and temperatures less than 150K;
- Liquid hydrogen vessels operating near 20K, that is the normal boiling point of H_2, and low pressures (less than 0.6MPa [12]).

These different storage solutions can be suitable or not depending on the key features requested by the particular application [12].

Compressed hydrogen

Compressed hydrogen (CGH_2) can be stored underground or in vessels. The first option is cheaper for large-scale storage and, therefore, is more suitable for applications that require considerable amounts of fuel. In these kinds of storage, hydrogen is usually kept at a pressure of around 20MPa. Some examples of this storage system can be found in Teeside, UK, and Texas, USA, where salt cavities are exploited for this purpose. Indeed, salt cavities are the most suitable option, and the only proven approach so far, for underground storage thanks to a number of reasons, like low construction costs, low leakage rates, and fast withdrawal and injection rates [11].

In the regions where salt cavities are not available, or in applications that don't require large amounts of fuel, like in the transport sector, hydrogen can be stored as compressed gas in tanks. Hydrogen vessels are usually cylindrical and can be divided into four different categories, as can be also seen in Figure 2.3:

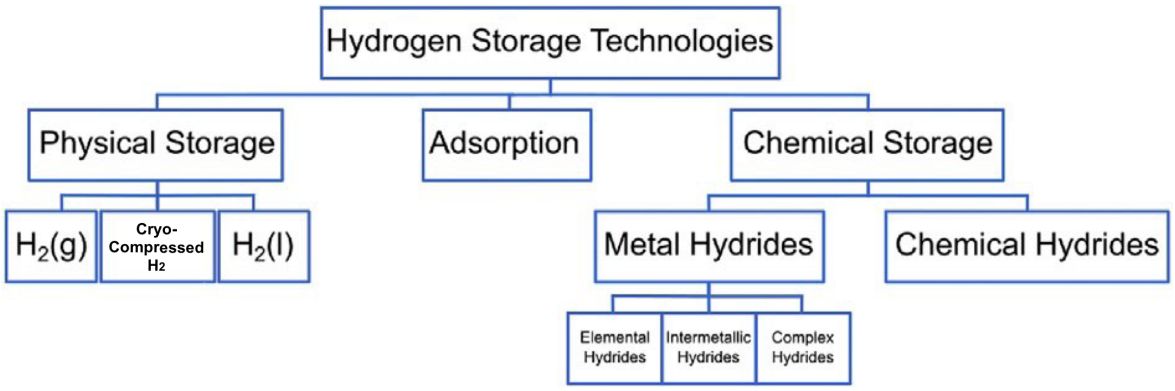

Figure 2.1: Categorization of hydrogen storage technologies (adapted from [11]).

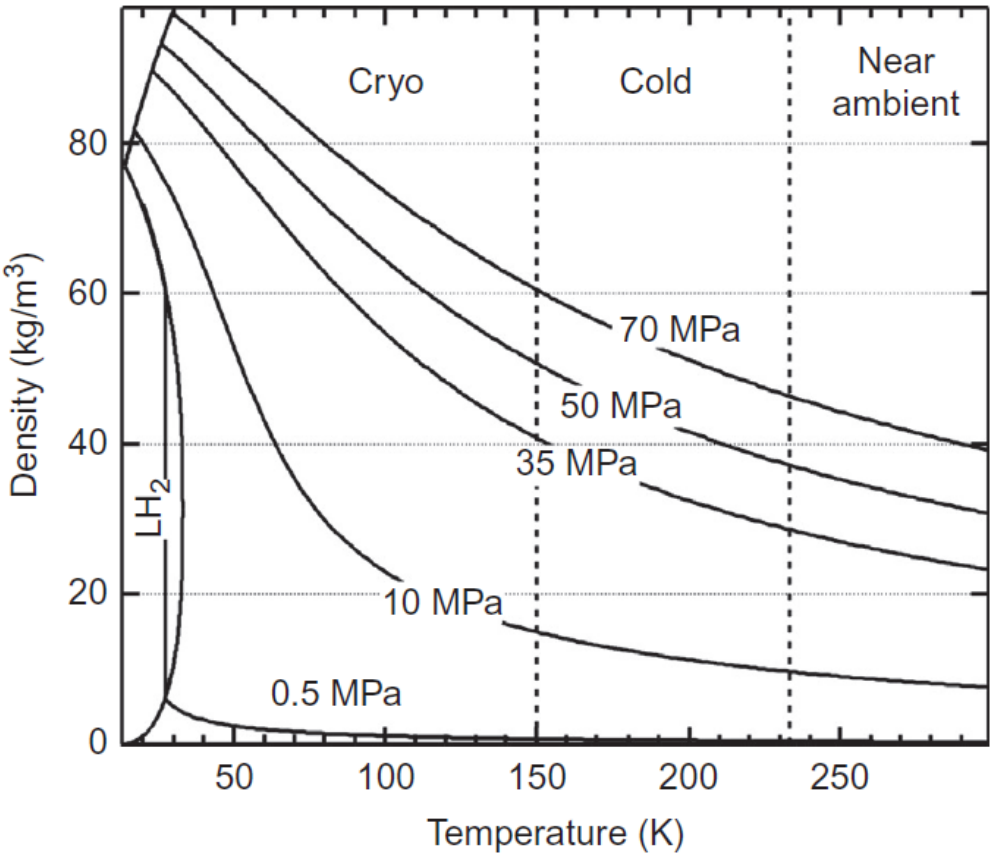

Figure 2.2: Hydrogen density versus temperature for several storage pressures [12].

- Type I – All-metal cylinders;
- Type II – All-metal hoop-wrapped composite cylinders;
- Type III – Fully wrapped composite cylinders with metallic liners;
- Type IV – Fully wrapped composite cylinders with nonload bearing nonmetallic liners [12].

In industrial applications, where the volume and the weight are usually a less stringent requirement compared to other fields, like the automotive sector, hydrogen is stored at 20-30MPa in type I tanks. Type II vessels, which allow higher storage pressures, are also used. These solutions are the cheapest, compared to the other kind of tanks, but have also the lowest mass storage efficiency, which is defined as the ratio between the mass of hydrogen contained in the tank and the mass of the vessel. For type I and II, the gravimetric storage efficiency (wt%) is around 1-2%. For this reason, in those sectors where weight and volume are more relevant aspects, such as in automotive applications, only type III or IV tanks can be used. Indeed, these types of vessels are made with lighter and particular materials and can stand pressures up to 45MPa for

type III cylinders and up to 70MPa for type IV tanks. Thus, the hydrogen capacities that can be delivered by these vessels are more than four times those of type I tanks [13].

Liquid hydrogen

Another way to increase hydrogen density is to liquefy it. The first who succeeded in hydrogen liquefaction was Dewar, who is also the inventor of the vacuum-insulated vessel, in 1898 [14]. Despite this early achievement, liquid hydrogen (LH_2) started to be commercially produced on a large scale only in the 1950s thanks to the increasing demand by the aerospace sector, as a propellant, and by the nuclear sector, for deuterium production [14].

The liquefaction process increases hydrogen density to 71kg/m^3 at atmospheric pressure and higher densities can be obtained by increasing the tank pressure [12]. On the other hand, hydrogen boiling point is 20K at ambient pressure and, thus, cryogenic temperatures are required to produce and store it [12]. Because of this, the liquefaction process is energy intensive and can consume up to 40% of the energy content [13]. Moreover, to maintain the hydrogen in a liquid phase, high-efficiency vacuum-insulated vessels are required. These tanks are composed of an inner pressure vessel and an outer jacket. The space in between is filled with super insulation materials and often vacuum-packed, in order to reduce conduction and irradiation heat losses, that would cause the boil-off, i.e., the evaporation of the liquid back into the gas phase [13].

In the liquefaction process, some reactions that involve hydrogen, like the ortho-to-parahydrogen conversion, take place. These reactions are highly exothermic and very slow and, for this reason, it is more effective to make them occur out of the vessel. Indeed, they are so exothermic that the energy released during the transformation process is high enough to vaporize the liquid hydrogen. Thus, to reduce energy consumption and the boil-off of liquid hydrogen, reactors with catalysts must be used for

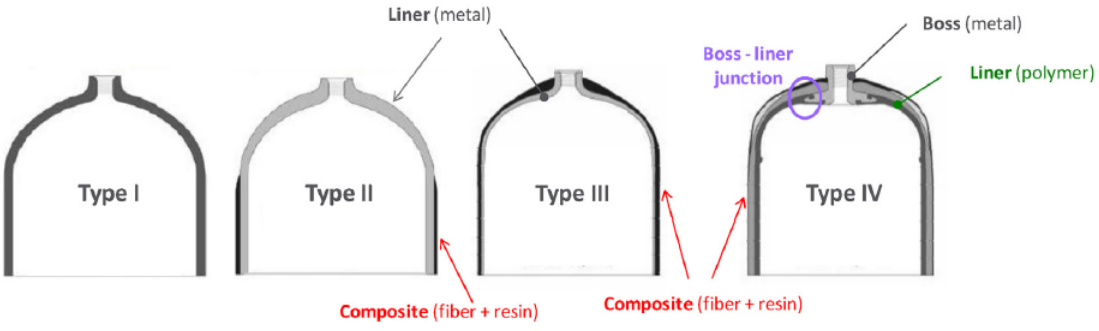

Figure 2.3: Representation of type I, II, III, and IV compressed gas storage vessels [13].

large-scale production facilities.

Despite these drawbacks, liquid hydrogen is a mature and proven technology and can reduce the problem of storage volumes. Furthermore, it is the most economic option when the transportation and storage of large quantities of hydrogen are required [14].

Cryo-compressed hydrogen

Another option is the cryo-compressed hydrogen storage (CcH_2), which is an in-between to compression at atmospheric temperature and liquefaction at ambient pressure. These types of vessels work with hydrogen at cryogenic temperatures, but with pressures up to 35MPa [15]. They can be used in a more flexible way since they can store hydrogen in different phase states: liquid hydrogen, supercritical cryogenic hydrogen, hydrogen in a two-phase region, and compressed hydrogen [15].

Their design is similar to the one of LH_2 tanks and it is shown in Figure 2.4. They're made with a Type III cryogenic inner vessel and an outer jacket that reduce the impact of the environment on the pressure vessel. The space in between is vacuumed and filled with insulation materials. The thickness of the insulation materials can be reduced compared to LH_2 storage tanks because the CcH2 vessels are less sensitive to heat transfer than the former [16]. This can lead to an improvement in storage density and efficiency.

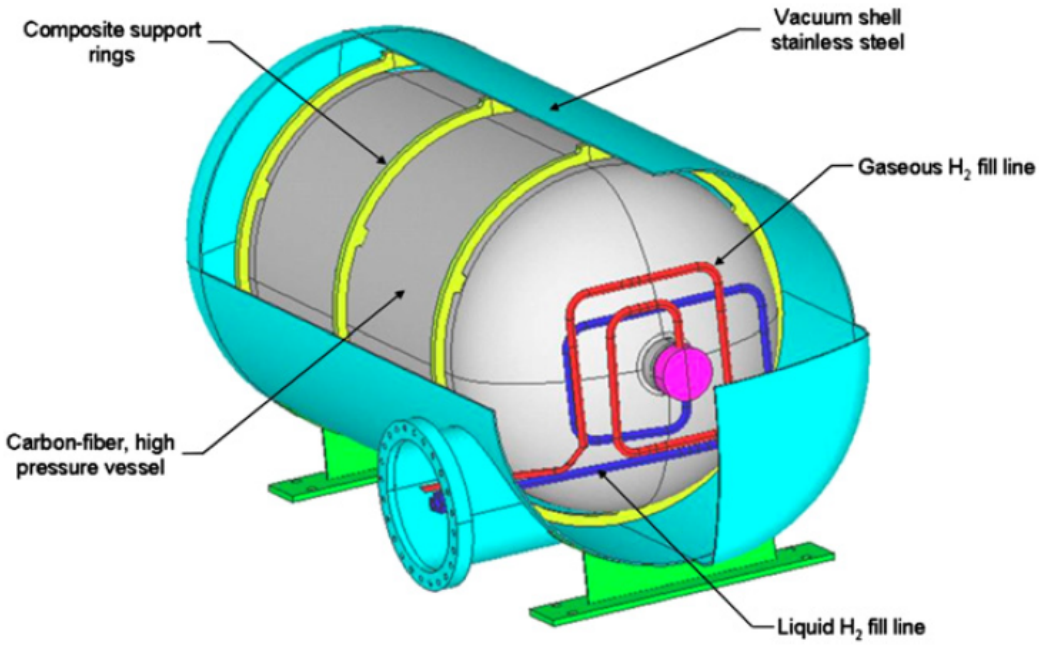

Figure 2.4: Generation 2 cryogenic capable pressure vessel design [16].

Another interesting aspect of these vessels is the increase in the dormancy period for

automotive applications. The ability of the tanks to stand higher pressures increases the time before the vaporized hydrogen is vented out of the vessel. Furthermore, if the vehicle is used, the hydrogen in the tank expands, reducing the inner pressure and contributing to cooling down the fuel and incrementing the dormancy period. Also, the risk of being stranded after a long-term parking period is avoided because, in the worst-case scenario, where the whole hydrogen is vaporized, 30% of the initial liquid content is still inside the tank in the gaseous phase.

Tests related to this storage system were accomplished by *Lawrence Livermore National Laboratory* (LLNL). They used a Type III cryogenic capable pressure vessel filled with 10.7kg LH_2 and they were able to drive the car for 1050km without refueling, that is the longest distance ever reached by a hydrogen vehicle. Now, other tests are being carried out with improved type III vessels, that might be able to increase the storage efficiency, thanks to a reduction in the volume of the tank [16].

2.1.2 Other storage systems

In addition to physical storage, other storage systems that exploit physical or chemical bonds are under investigation. Storage by adsorption exploits the weak physical van der Waals bonds to store hydrogen in porous materials with a high specific area, like porous polymeric materials, zeolites, and carbon-based porous materials (e.g., carbon nanotubes). High pressures and low temperatures are needed to achieve high storage densities and, therefore, one of the biggest issues is related to heat removal. Indeed, high quantities of liquid nitrogen are requested since the adsorption reactions are exothermic. For these reasons, nowadays these storage systems exist only at laboratory scales [11].

The other way to store hydrogen is by exploiting chemical bonds, in metal or chemical hydrides. The first solution requires the hydrogen to be stored in solid compounds, i.e., metal hydrides, resulting in high-density storage composites. The main drawback of this solution is the high temperature requested for the dehydrogenation process. Indeed, a heat source is needed to break the chemical bonds and re-obtain the pure hydrogen.

The other option consists in forming chemical hydrides, mostly in a liquid phase, like ammonia or methanol. These compounds are already largely used nowadays in the chemical industry and present high storage densities. The main issue is related to the fact that these compounds are toxic, so, strict safety rules are needed. On the other hand, in this case, the dehydrogenation process could be avoided if these compounds are directly used as fuels [11]. As a comparison, in Figure 2.5 the storage densities of the main storage systems are shown.

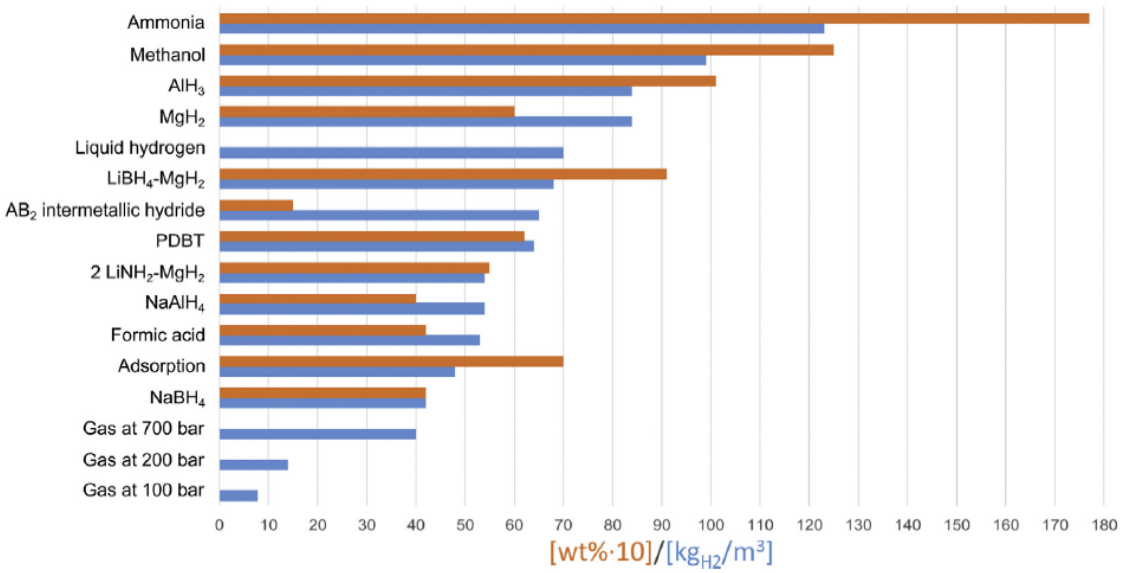

Figure 2.5: Volumetric (kg/m^3, in blue) and gravimetric (wt% multiplied by ten, in orange) hydrogen storage densities of considered technologies [11].

2.2 Loss of containment in hydrogen equipment

When considering the construction of a new facility, like a hydrogen storage plant, safety has to be taken into account. The loss of containment (LOC), also called loss of physical integrity (LPI), is a critical event that consists of a mechanical and physical failure of equipment and can lead to damage to people or objects.

The issues involved in a safety analysis can be summarized by the bow-tie diagram in Figure 2.6. The hazard is defined as a "source of danger" and, in the case of hydrogen, it is attributable to its chemical and physical properties, mainly related to its high flammability, both in the liquid and gaseous phase. It is different from the risk, which is linked to the possibility of a critical event or injury to occur and, thus, it considers the probability of a hazard to be converted into damage [7]. The fault events are all the causes that can lead to a LOC event and will be discussed in this section. The consequences, that will be described in the next section, are the damages caused by the critical events [7].

2.2.1 Hydrogen Damages

Defining all the aspects related to a critical event is key to completely understanding the process and defining an inspection and maintenance plan that fits the application. However, when hydrogen is present, a lot of uncertainties related to LOC causes are still present and affect the risk analysis of hydrogen technologies, as described in literature [17, 18]. Indeed, even if hydrogen is known to affect the characteristics and integrity

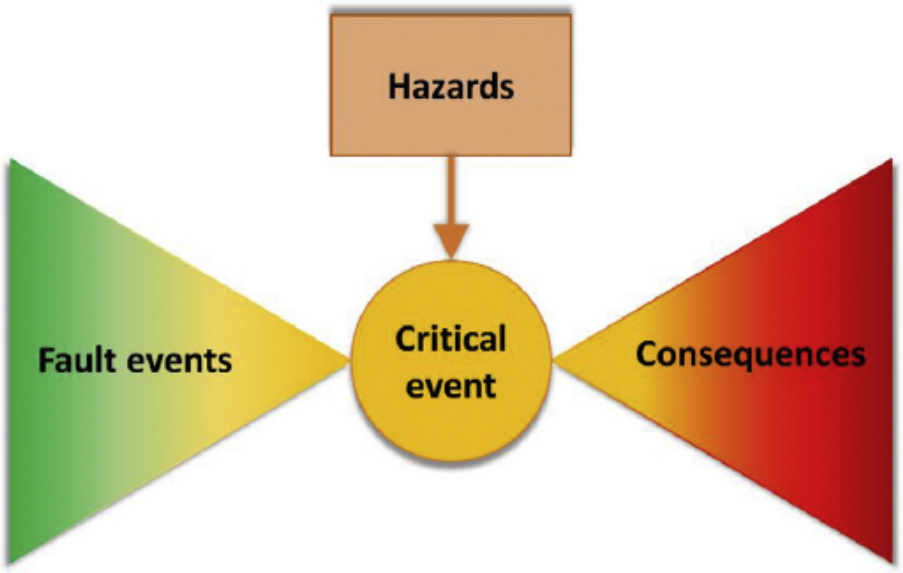

Figure 2.6: Bow-tie approach adopted to describe the hydrogen safety aspects [7].

of the materials used for its confinement, the mechanisms involved in the degradation processes, called hydrogen damages (HDs), are not completely understood yet.

The manifestation of the hydrogen-induced degradation phenomena is connected to the combination of three different factors:

- Environment: hydrogen amount, form, and processes;
- Field type: mechanical, electrochemical, and operating conditions;
- Material: chemical and physical characteristics.

If not taken into account, the synergy of these factors can lead to the LOC of hydrogen equipment [7].

Multiple types of HDs have been recognized and they are usually classified as follows:

- Hydrogen embrittlement
- Hydrogen blistering
- High-temperature hydrogen attack
- Metal hydride formation

Some of these processes are illustrated in Figure 2.7.

Hydrogen embrittlement is a form of degradation that lowers the strength of material via the absorption and permeation of hydrogen [19]. This term is referred to

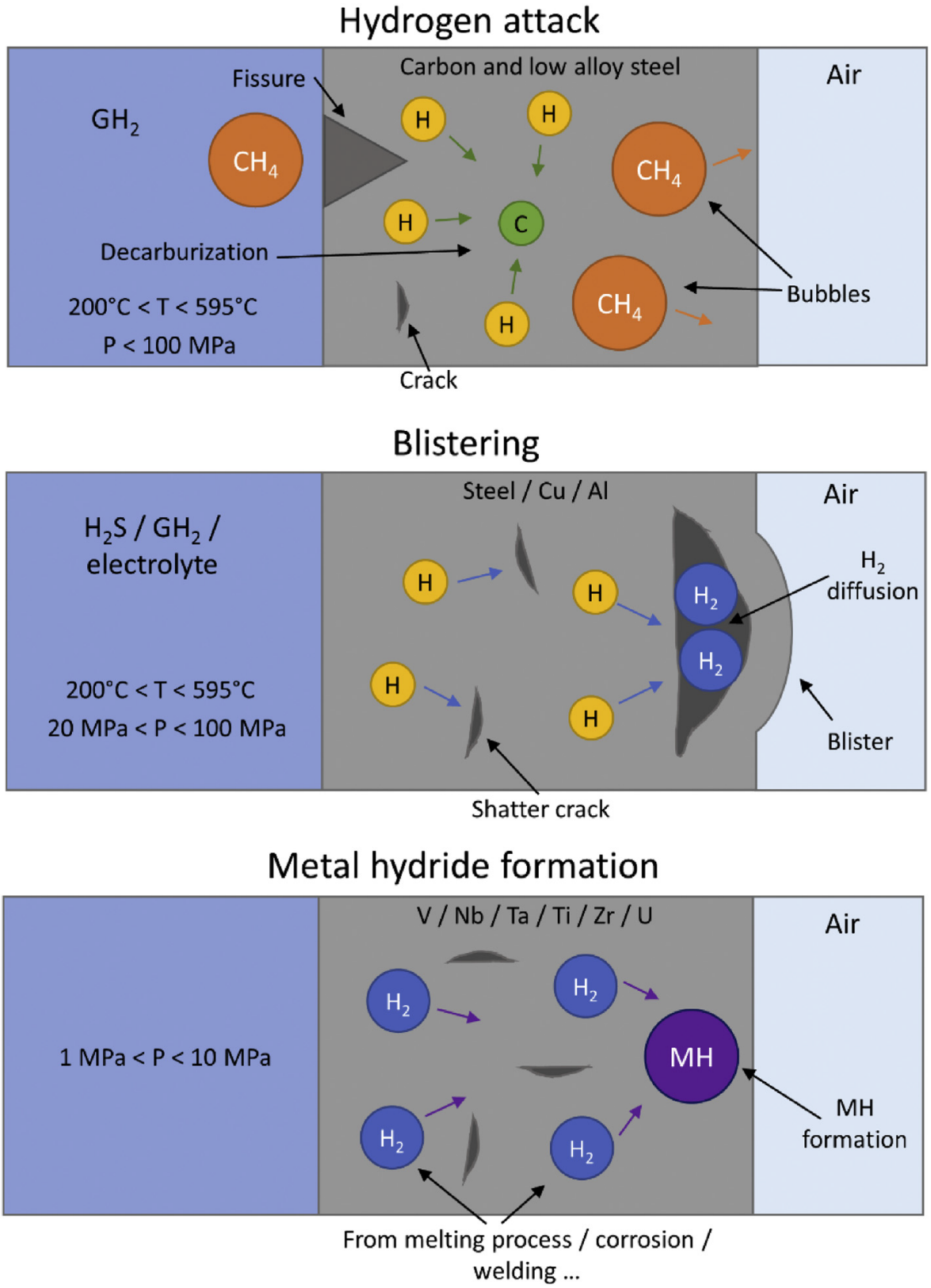

Figure 2.7: Schematic of hydrogen attack, blistering, and metal hydride formation phenomena [7].

a category of phenomena that includes hydrogen environmental embrittlement (HEE) and hydrogen stress cracking (HSC) [20]. HEE takes place during the plastic deformation of alloys in contact with gasses characterized by a high hydrogen concentration. It affects the materials with a low hydrogen solubility and is more intense at ambient temperature and when pure-hydrogen and high-pressure are involved [7]. HSC is described by the brittle fracture of a normally ductile alloy under a constant load in an H_2 environment. This type of HD is linked to the absorption of hydrogen and a delayed time to failure, due to the time needed by the gas atoms to diffuse toward regions of high triaxial stress. It usually results in sharp and singular cracks that could lead to the catastrophic failure of the equipment [20].

Hydrogen blistering mainly occurs in low-strength alloys and is enhanced by the presence of corrosive substances, like H_2S. It is related to the diffusion of atomic hydrogen into internal defects, where it precipitates as molecular hydrogen. This process leads to localized high pressure, causing plastic deformations, referred to as blisters, that often rupture [7].

High-temperature hydrogen attack takes place in carbon and low-alloy steels exposed to high-pressure hydrogen and high temperatures, over 200°C, for a prolonged time [20]. In this case, hydrogen enters the metal and interacts with the material to form insoluble products, like methane. This reaction occurs at the grain boundaries and causes high localized pressure and the decarbonization of the metal, resulting in a reduction in its strength [21].

Finally, metal hydride formation is the cause of degradation in mechanical properties of metals containing magnesium, zirconium, titanium, niobium, tantalum, vanadium, and their alloys and it's due to the precipitation of the metal hydride phases [20].

It is acknowledged that the effects of hydrogen damages are related to a wide range of factors, such as pressure, temperature, exposure time, hydrogen concentration, properties of the material, etc. Nevertheless, even if several research has been carried out over the decades and a considerable number of theories have been proposed to describe HDs, still none of them can fully explain and predict the material's behavior when exposed to hydrogen [19].

2.2.2 Thermal and mechanical stress

Besides the hydrogen damages, previously described, other factors can affect material health. The operating conditions in which the tank has to operate can indeed provoke thermal and mechanical stresses to it and, therefore, be the cause of component failure. Because of this, thermal gradients, dimensional change, and material behavior during fatigue cycles have to be taken into account during the design phase.

When the hydrogen is stored in its liquid phase and, thus, the temperatures are cryogenic, thermal stress could have relevant effects on the equipment. In these cases, the difference in temperature is unavoidable and so, thermal gradients are present on various components of the facility both at steady-state and during transient, such as the filling and the emptying of the tank. Since hydrogen has a low boiling point, to reduce this kind of stress a pre-cooling process with liquid nitrogen or other cryogenic substances is needed [7].

Another type of stress caused by low temperatures is due to the change in the dimensions of the tank. Indeed, most of the materials face a reduction in dimension by decreasing the temperature. To prevent the severe potential consequences of this effect, the parts of the vessel affected by this problem have to be free to expand and contract without causing irreversible changes in the tank characteristics [7].

In addition to the thermal stress, also fatigue cycles can affect the material life. This aspect is of crucial importance for the correct functioning of the instrumentation and to avoid early failure of the equipment. The study of fatigue cycles in a hydrogen environment is still lacking a deep understanding, hence it has to be evaluated case-by-case [7].

2.3 Loss of containment consequences

As described before, there are many causes that can reduce the strength and the life of hydrogen vessels. If not considered properly, those processes can lead to a loss of containment and, thus, to multiple consequences. In the following, an overview of the different types of aftermaths is presented, focusing more on the phenomena of Boiling Liquid Expanding Vapor Explosion (BLEVE) and Pressure Vessel Burst (PVB).

2.3.1 Boiling Liquid Expanding Vapor Explosion

The Boiling Liquid Expanding Vapor Explosion, referred as BLEVE, is an atypical accident scenario, i.e., "a scenario deviating from normal expectations of unwanted events or worst case reference scenarios and, thus, not deemed credible by the common processes applied for risk assessment" [22], that normally presents extremely severe consequences, even if they are very unlikely to happen, as reported in [23].

The first definition of BLEVE was made in 1957 by J.B. Smith, W.S. Marsh, and W.L. Walls, three workers of the Factory Mutual Research Corporation [24]. Since then, different definitions of this accident were proposed and, nowadays, the current definition is the one made by Casal [25]: "A BLEVE is the explosion of a vessel containing a liquid (or liquid plus vapor) at a temperature significantly above its boiling point at atmospheric pressure". According to this definition, every tank containing

liquid, or liquefied gas, that fails might go through a BLEVE if its content is superheated, regardless of the type of substance. Indeed, this accident occurred also for inert substances like water, nitrogen, and carbon dioxide, as reported in Table 2.1 [24, 26].

Description of a BLEVE accident

A BLEVE event starts with the failure of a pressurized vessel filled with a liquid at a temperature above its boiling point at atmospheric pressure. The rupture can be originated both from thermal or mechanical causes. In the first case, due, for example, to the engulfment of the tank in a fire, the BLEVE is referred to as "fired" or "hot BLEVE". Otherwise, if it is originated from different causes, like a violent impact, it is defined as "cold BLEVE" [26]. Another classification of BLEVEs accidents is based on the way the tank fails: single and two-step BLEVEs. The single-step BLEVE is originated if the vessel is ruptured completely and instantaneously, while the two-step BLEVE occurs when the tank failure time is in the range of 2 s. It seems that the two-step BLEVE results in a more severe blast overpressure when compared to the single-step one [27].

The main stages that are observed in a BLEVE accident are provided in [24] and presented below:

1) A container filled with a pressurized liquid gas, like LH_2, is stressed by a thermal load or is damaged by a violent impact, fatigue or corrosion;

2) The tank fails;

3) The vessel undergoes an instantaneous depressurization and a subsequent explosion;

4) The tank is broken into pieces and the debris is propelled outward by the overpressure waves;

5) If the substance in the vessel is flammable or toxic, a fireball or a toxic dispersion takes place.

As mentioned, the main consequences of a BLEVE accident are the overpressure waves, the missiles generated from the tank shattering, and, in the case of a flammable substance, a fireball. Different models have been proposed to predict consequences behaviors, as can be seen in [28, 29], and in the next section, the fireball models will be presented in more detail.

Table 2.1: List of BLEVE accidents in the period 1926-2004 [24, 26].

Substance	**Type**	**No. of accidents**	**Casualties**	**Injured**
Propane	Flammable	24	121	7761
LPG	Flammable	17	12	35127
Chlorine	Toxic	7	139	-
Ammonia	Toxic	6	55	25
Butane	Flammable	5	394	7510
Gasoline	Flammable	3	10	2
Acrolein	Flammable	2	-	-
Carbon dioxide	Non-flammable Non-toxic	2	9	-
Ethylene oxide	Flammable	2	1	5
LNG	Flammable	2	14	76
Propylene	Flammable	2	213	-
Vinil chloride	Flammable Toxic	2	1	50
Borane tetrahydrofuran	Flammable Toxic	1	-	2
Butadiene	Flammable Toxic	1	57	-
Chlorobutadiene	Toxic	1	3	-
Ethyl ether	Flammable	1	209	-
Hydrogen	Flammable	1	7	-
Isobutene	Flammable	1	-	1
Maltodextrin	Toxic	1	-	-
Methil bromide	Toxic	1	2	-
Nitrogen	Non-flammable Non-toxic	1	2	-
Phosgene	Toxic	1	11	171
Steam	Non-flammable Non-toxic	1	4	7
Water	Non-flammable Non-toxic	1	7	-

Superheat limit theory

One of the main prerequisites to classify an explosion as a BLEVE is the superheat status of the liquid phase. The superheat limit theory was proposed for the first time by Reid in 1976 [30] and tries to determine the conditions under which a BLEVE can occur. According to this theory, there is a temperature, called superheat limit temperature (T_{SL}), above which the liquid phase cannot exist anymore. This limit varies depending on the substance considered and the pressure of the tank. Thus, if the substance temperature goes beyond the T_{SL} at a given pressure, homogeneous nucleation is triggered and the liquid starts boiling violently, provoking the physical explosion of the vessel [26].

There are two different ways to reach the T_{SL}: at constant pressure or at constant temperature. At constant pressure, it can be attained by heating the liquid until the threshold is reached and the liquid starts the homogeneous nucleation. At constant temperature, the superheat limit can be attained if the liquid, contained in a pressurized vessel, quickly depressurizes because of some kind of tank failure. In this second case, the liquid temperature suddenly becomes higher than its boiling point because of the new reduced pressure [28].

In order to calculate the T_{SL}, different methods have been proposed. The first one, and still the more widely used, is the one proposed by Reid and consists of a correlation with the critical temperature (T_C) [30]:

$$T_{SL} = 0.895 \cdot T_C \tag{2.1}$$

In the case of hydrogen, the critical temperature is $T_C = 32.938K$ [10]. This equation was obtained by experiments on bubble-column at different pressure and with various substances: di-chlorodifluoromethane, n-pentane, n-hexane, n-heptane, and cyclohexane [30].

Other more recent methods were proposed to evaluate the T_{SL}. One of these methods estimates the superheat limit temperature from the tangent to the saturation curve at the critical point [31]. This method results in one of the most conservative temperature estimations. To evaluate the T_{SL}, the tangent can be built graphically to avoid the errors that the Clausius-Clapeyron equation presents next to the critical point. In this way, the T_{SL} is the temperature intercepted by the tangent at atmospheric pressure (P_0) [32].

A third method was proposed in [33] and estimates the T_{SL} by an energy balance. In this case, an adiabatic vaporization is considered after the depressurization of the tank. During this process, a part of the liquid cools down to the boiling point at atmospheric pressure. While the liquid cools down, it releases some heat, that can be absorbed by another part of the liquid, leading to its vaporization. The superheat limit temperature is the temperature at which the heat released by 50% of the liquid is

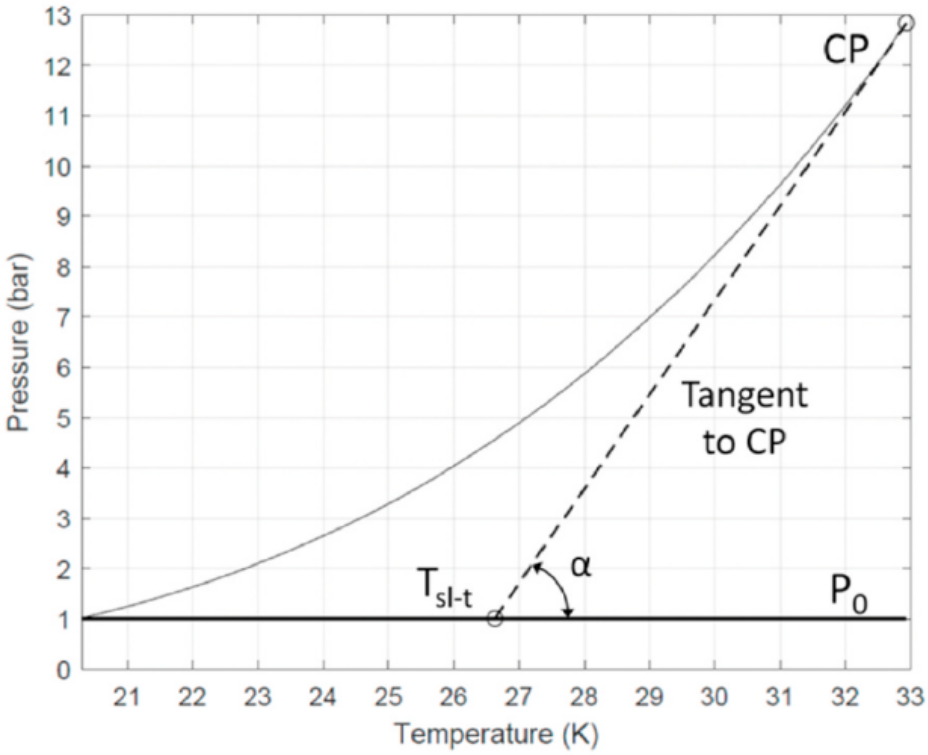

Figure 2.8: T_{SL} calculated with the tangent to the saturation curve [32].

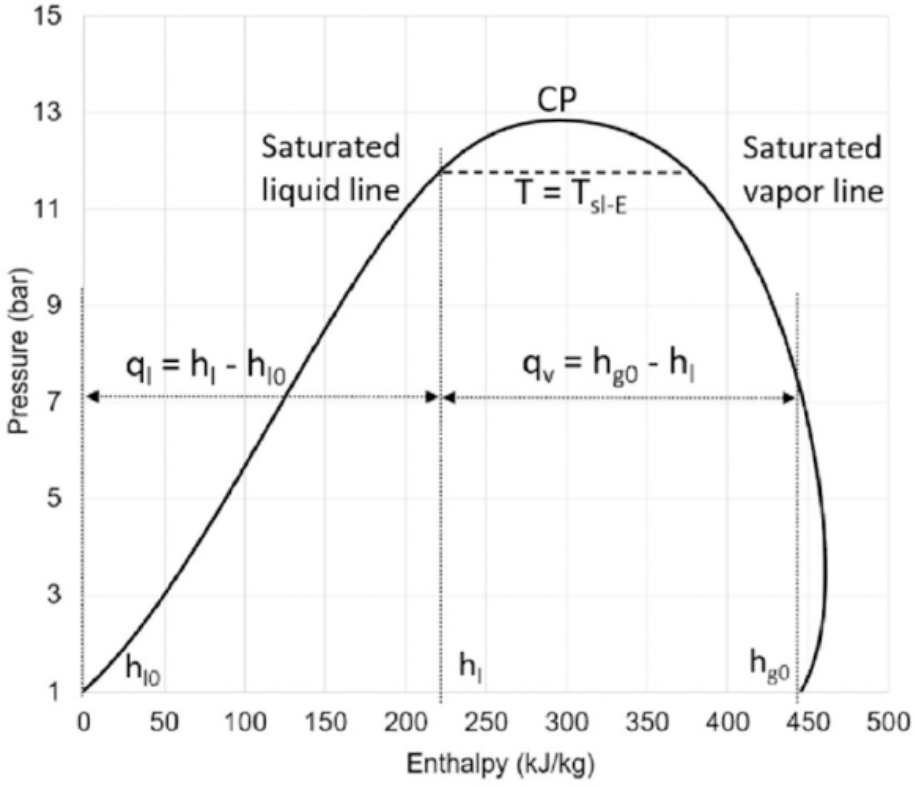

Figure 2.9: T_{SL} calculated with the energy balance equation [32].

equivalent to the heat needed by the other half of the liquid to vaporize, as described in [32]. Figure 2.8 and Figure 2.9 show the methods here described.

As previously mentioned, the T_{SL} is an important parameter to evaluate if an accident is to be considered a BLEVE or not. However, this does not imply that an explosion cannot occur if the temperature of the liquid is lower than the superheat limit temperature. Indeed, the liquid could be in a metastable state and, because of a tank failure, it can start flashing through heterogeneous nucleation, generating a detonation. In this case, the consequent explosion is less severe compared to BLEVE, since the homogeneous nucleation is a stronger process [26].

2.3.2 Pressure Vessel Burst

Similar in the effects, but different on the initial condition, is the pressure vessel burst, abbreviated in PVB. It is "a type of explosion that involves burst of a pressure vessel containing gas at elevated pressure" [29]. Despite this definition, also vessels containing liquid can undergo PVB, provided that the liquid does not change phase during the depressurization process. Indeed, if the liquid starts flashing after the tank rupture, the explosion is referred to as BLEVE, and is described in the previous part of this section. As for BLEVEs, the vessel content does not have to be either flammable or reactive to go through a PVB accident.

In the last century, safety standards were improved a lot, in order to reduce PVB frequency. In fact, before the 1900s, PVB was a usual phenomenon. For this reason, new standards regarding the design and manufacture of pressure tanks were introduced both in USA and Europe and are now widely used worldwide. High safety margins are now required and, thus, the pressure vessel has to stand up to 2.4 or 4 times the design maximum allowable working pressure (MAWP), depending on the code considered [29].

Regardless of these new standards, PVBs still occur sometimes, because of a variety of reasons:

- Loss of containment, due to corrosion, fatigue, or other processes that weaken the vessel materials, like the hydrogen damages;
- Pressurization over the ultimate failure pressure, caused by some internal process, like chemical reactions, or pressure relief valves failure, not allowing an appropriate pressure reduction;
- External factors, that compromise mechanical integrity, such as a violent impact or overheating due to fire exposure;
- Fabrication, transportation, and installation defects, that reduce the tank strength below the design targets.

Similarly to BLEVE, the main aftermaths of a PVB accident are the pressure wave, the missiles generated from the tanks shattering and, in case of a flammable content, a fireball. The blast effects are the main source of damage in PVB, while fragments usually can harm in a relatively close space. Finally, the thermal hazard that results from PVB is generally minor to negligible when compared to the one caused by BLEVEs accidents [29].

2.3.3 Continuous releases

The two phenomena of BLEVE and PVB just described are related to the consequences of instantaneous releases of fuel, due to a sudden burst of the storage vessel. In addition to them, other aftermaths, related to continuous releases, are possible. In this second case, the fuel, and in particular H_2, spills out from the tank without any vessel blast.

Hydrogen is a small molecule. This characteristic can allow it to leak from microscopic holes that might be present on the equipment. Even if it's not a toxic gas, the spill in a close environment could be dangerous to people because it might cause asphyxiation. Indeed, the H_2 molecules replace oxygen, becoming dangerous if its concentration in air is reduced below 19.5% by volume [34]. Furthermore, the ignition of leaked hydrogen is very likely to occur because of its wide range of flammability (4-75% of concentration in volume [6]) and its low ignition energy (0.017mJ [5]), driving to more hazardous aftermath. Depending on the type of release, different consequences can be identified. In Figure 2.10 the event tree of releases from hydrogen liquid tanks is presented.

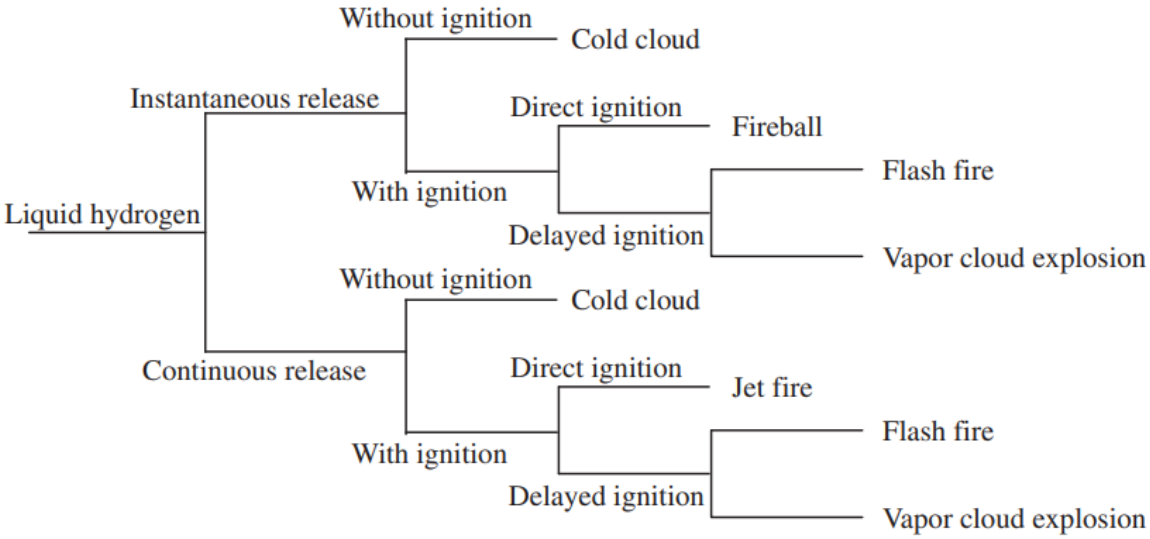

Figure 2.10: Event tree of releases from liquid hydrogen tank [35].

If the release involves LH_2, a two-phase mixture is dispersed in the surrounding, developing a cold cloud. This might cause damage to equipment and structures or

harm to people in the nearby because of its low temperatures, resulting in cryogenic burns to people [35]. For the gaseous hydrogen, the cold cloud cannot occur, but the asphyxiation hazard is still to be considered.

In the event ignition takes place, different types of combustion processes can occur based on whether ignition is instantaneous or delayed. If the ignition is immediate, a jet fire develops. Jet fires are high-velocity turbulent flames generated by the combustion of fuel released in a certain direction and with considerable momentum. If the gas is stored in pressurized tanks, the momentum is due to the difference in pressure between the inside of the tank and the surrounding ambient [34].

Otherwise, if the ignition is delayed, hydrogen has enough time to mix with the ambient air before the combustion starts, leading sometimes to an explosion. In this case, the consequences can be flash fire or a vapor cloud explosion (VCE), depending on the release conditions. Between them, VCE is deemed to have the most dangerous effects and, therefore, it is the one to be considered while evaluating the safety distances [34].

2.4 Fireball analysis

As previously described, a fireball is a common aftermath when a flammable substance is involved in vessel failure. In this section, firstly the fireball event is described. Then, the main analytical models found in the literature and used to predict fireball behavior are presented.

2.4.1 Fireball theory

The Yellow book defines a fireball as a "fire, burning sufficiently rapidly for the burning mass to rise into the air as a cloud or ball" [36]. The fireball differs from the other combustion events, like flash fire or vapor cloud explosion, by the fact that the ignition precedes the mixing with the surrounding air. For this reason, the entrainment and the mixing of the fuel with the air happen as the burning takes place [28]. Thanks to the high turbulence of the process, there is usually a small portion of un-combusted fuel or soot in the nearby of fireball. The combustion, that is from the outside inward, results in the rising of the fireball and in its dimensions growth [37]. In Figure 2.11 an example of a fireball resulting from an induced liquefied natural gas (LNG) BLEVE can be seen.

The evolution of fireball dimension during time is presented in Figure 2.12. After the ignition, three different stages for fireball development can be distinguished [39]:

Figure 2.11: Flashing cloud (left) and fireball (right) resulting from and induced LNG BLEVE [38].

1) *Fireball growth.* During this phase, the combustion takes place in the external part of the fireball, where the fuel is in contact with the air. The heating provokes a rapid volume growth, enhancing also the mixing of fuel and air;

2) *Steady combustion.* All the fuel mass burns and the fireball lifts off thanks to buoyancy effects, giving to it the typical "mushroom shape". The fireball dimension is almost constant during this phase;

3) *Fireball extinction.* All the flammable substance is consumed and the fireball temperature starts decreasing rapidly. The dimension can either increase or decrease depending on the actual combustion conditions.

Fireball temperature varies a lot during the entire combustion process and it is usually within the range of 900°C to 1200°C. The color of the fireball depends on how the soot particles that are involved in the fireball react at the combustion temperature [37].

2.4.2 Fireball models

If the tank is filled with a great amount of fuel, the fireball derived from the vessel failure can often result in damage to people and structures at greater distances than the blast waves. For this reason, trying to predict the heat radiation generated from the fireball and its effects is of great importance, in order to ensure the safety parameters required. The main aspects needed to calculate the heat radiation are:

- Fireball diameter;
- Fireball duration;

- Fireball surface emissive power (SEP).

Over the years, several analytical models have been proposed and are hereby presented [29].

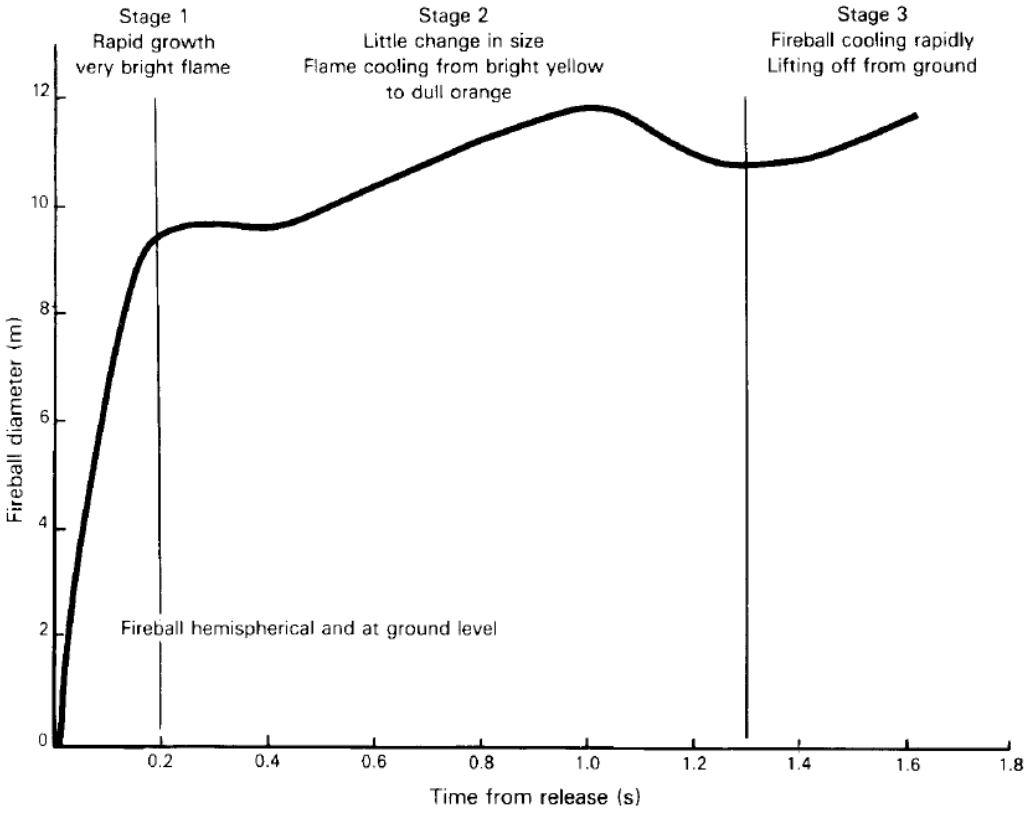

Figure 2.12: Fireball development as a function of time [39].

Fireball dimension and duration

A lot of experiments have been made to measure the size and duration of fireballs generated from different fuels. From these tests, many empirical correlations have been proposed, relating the fuel mass involved in the fireball to the diameter and duration, and are presented in Table 2.2. Among all these relationships, the most used for the diameter is the one proposed by Roberts [39]:

$$D = 5.8 \cdot m_f^{1/3} \tag{2.2}$$

where m_f is the fuel mass in kg and D is the calculated fireball diameter in m. The analytical models used to estimate the fireball duration vary on the type of fireball considered:

- Momentum-driven fireball;

- Buoyancy-driven fireball.

It is of common use to consider the momentum-driven formula for fuel masses lower than 30,000kg and the buoyancy-driven formula for fuel masses above 30,000kg [29]. The equations used in these cases are respectively:

$$t = 0.45 \cdot m_f^{1/3} \text{ for } m_f < 30,000kg \tag{2.3}$$

$$t = 2.60 \cdot m_f^{1/6} \text{ for } m_f > 30,000kg \tag{2.4}$$

In particular, for the momentum-driven case the durations are assumed to be in the range between $0.45 \cdot m_f^{1/3}$ and $0.9 \cdot m_f^{1/3}$ [38]. Also, the time at which lift-off is considered to occur is 1/3 of the total duration of the fireball (i.e., $t_{lo} = t/3$) [40].

Heat radiation

The heat radiation can be calculated through the solid flame model, according to this equation:

$$q = \text{SEP} \cdot F \cdot \tau_a \tag{2.5}$$

where q is the radiation received by the target in W/m^2, SEP is the surface emissive power in W/m^2, F is the view factor and τ_a is the atmospheric transmissivity [29].

Surface emissive power The SEP is the radiative heat flux emitted from the fireball surface and can be determined by experimental tests. It can also be estimated with two different theoretical relations. The first one is the Stefan-Boltzmann's law:

$$\text{SEP} = \varepsilon \cdot \sigma \cdot T^4 \tag{2.6}$$

where ε is the emissivity of the fireball, σ is the Stefan-Boltzmann's constant, that is equal to $5.67 \times 10^{-8} W/(m^2 K^4)$, and T is the flame temperature in K [41].

The other way to estimate the SEP value is using the following equation [42]:

$$\text{SEP} = \eta \cdot \frac{m_f \cdot \Delta H_c}{\pi \cdot D^2 \cdot t} \tag{2.7}$$

where η is the fraction of total heat radiated from the fireball, m$_f$ is the fuel mass, ΔH_c is the heat of combustion of the fuel, D is the fireball diameter and t is the fireball duration. The variable η usually assumes values between 25% and 40% and can be calculated from Equation (2.8), where P is the pressure at which the tank bursts [42]:

$$\eta = 0.00325 \cdot P^{0.32} (P < 6 \cdot 10^6 Pa) \tag{2.8}$$

From experimental tests, it is known that the SEP value usually ranges between 200 and 400 kW/m^2, and a value of 350 kW/m^2 is considered reasonable for the majority of hydrocarbons [42].

Table 2.2: Empirical relationships for fireball durations and diameters [24, 29].

Source **Empirical correlation**	**Material**	**Diameter [m]**	**Duration [s]**
Hardee and Lee 1973	Propane	$5.55 \cdot m_f^{0.333}$	-
Fay and Lewis 1977	Propane	$6.28 \cdot m_f^{0.333}$	$2.53 \cdot m_f^{0.167}$
Hasegawa and Sato 1977	Propane	$5.28 \cdot m_f^{0.277}$	$1.10 \cdot m_f^{0.097}$
Hasegawa and Sato 1978	n-Pentane	$5.25 \cdot m_f^{0.314}$	$1.07 \cdot m_f^{0.181}$
Williamson and Mann 1981	Not provided	$5.88 \cdot m_f^{0.333}$	$1.09 \cdot m_f^{0.167}$
Lihou and Maund 1982	Butane	$5.72 \cdot m_f^{0.333}$	$0.45 \cdot m_f^{0.333}$
Lihou and Maund 1982	Rocket Fuel	$6.20 \cdot m_f^{0.320}$	$0.49 \cdot m_f^{0.320}$
Lihou and Maund 1982	Propylene	$3.51 \cdot m_f^{0.333}$	$0.32 \cdot m_f^{0.333}$
Lihou and Maund 1982	Methane	$6.36 \cdot m_f^{0.325}$	$2.57 \cdot m_f^{0.167}$
Moorhouse and Pritchard 1982	Flammable Liquid	$5.33 \cdot m_f^{0.327}$	$1.09 \cdot m_f^{0.327}$
Lihou and Maund 1982	Propane	$3.46 \cdot m_f^{0.333}$	$0.31 \cdot m_f^{0.333}$
Duiser 1985	Flammable Liquid	$5.45 \cdot m_f^{1.3}$	$1.34 \cdot m_f^{0.167}$
Marshall 1987	Hydrocarbon	$5.50 \cdot m_f^{0.333}$	$0.38 \cdot m_f^{0.333}$
Gayle and Bransford 1965, Bagster and Pitblado 1989	Flammable Liquid	$6.14 \cdot m_f^{0.325}$	$0.41 \cdot m_f^{0.340}$
Pietersen 1985, CCPS 1989, Prugh 1994, TNO 1997	Flammable Liquid	$6.48 \cdot m_f^{0.325}$	$0.852 \cdot m_f^{0.260}$
Roberts 1982, CCPS 1999	Flammable Liquid	$5.80 \cdot m_f^{0.333}$	$0.45 \cdot m_f^{0.333}$ $(m_f < 30,000kg)$
Roberts 1982, CCPS 1999	Flammable Liquid	$5.80 \cdot m_f^{0.333}$	$2.60 \cdot m_f^{0.167}$ $(m_f > 30,000kg)$
Martinsen and Marx 1999	Flammable Liquid	$8.66 \cdot m_f^{0.25} t^{0.333}$ $(0 \leq t \leq t_b/3)$	$0.9 \cdot m_f^{0.25}$

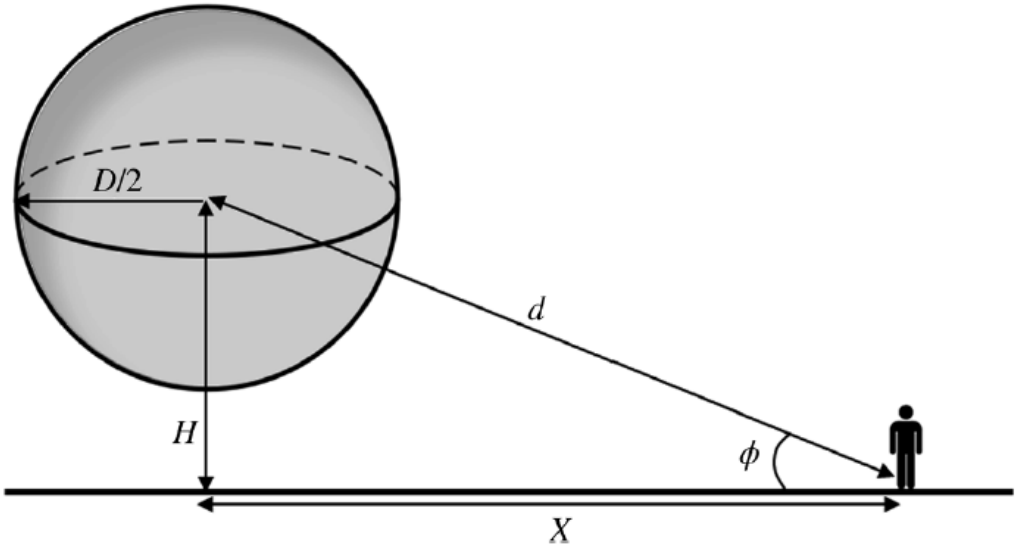

Figure 2.13: Fireball geometry and position with respect to a given target [42].

View factor The view factor F associates the radiation received from the target with the surface emissive power of the fireball. It can be calculated with the Equation (2.9) if the horizontal distance between the fireball and the target X is longer than the fireball radius $D/2$:

$$F = \left(\frac{D}{2d}\right)^2 \cdot \cos(\theta) \tag{2.9}$$

in which θ is the angle between the normal to the target surface and the fireball axis. For conservative reasons, this angle is often considered equal to zero [41]. In Figure 2.13 the different geometry parameters considered in the fireball event are shown.

To calculate the distance d between the target and the fireball center, the height H of the fireball is required. Depending on the authors, the fireball is assumed to be always in contact with the ground, and therefore $H = D/2$, or it lifts off reaching a height equal to one-and-a-half times its radius, and thus $H = 0.75 \cdot D$ [42]. Still, other authors suggested a maximum height corresponding to its maximum diameter ($H = D$) [41].

Atmospheric transmissivity Finally, multiple equations have been proposed to calculate the atmospheric transmissivity [42]:

$$\text{for } P_w \cdot \left(d - \frac{D}{2}\right) < 10^4 N/m: \qquad \tau_a = 1.53 \cdot \left(P_w \cdot \left(d - \frac{D}{2}\right)\right)^{-0.06} \tag{2.10}$$

$$\text{for } 10^4 \leq P_w \cdot \left(d - \frac{D}{2}\right) \leq 10^5 N/m: \qquad \tau_a = 2.02 \cdot \left(P_w \cdot \left(d - \frac{D}{2}\right)\right)^{-0.09} \tag{2.11}$$

$$\text{for } P_w \cdot \left(d - \frac{D}{2}\right) > 10^5 N/m: \qquad \tau_a = 2.85 \cdot \left(P_w \cdot \left(d - \frac{D}{2}\right)\right)^{-0.12} \tag{2.12}$$

where P_w is the partial pressure of water in the atmosphere, that depends on the ambient temperature (T_0) and relative humidity (RH):

$$P_w = \frac{RH}{100} \cdot e^{\left[23.18986 - \frac{3816.42}{T_0 - 46.13}\right]} \tag{2.13}$$

Also, another equation proposed by CCPS [29] can be used to estimate τ_a:

$$\tau_a = \log\left[14.1 \cdot RH^{-0.108} \cdot \left(d - \frac{D}{2}\right)^{-0.13}\right] \tag{2.14}$$

Thermal dose Once the heat radiation is calculated, the thermal dose, in the following abbreviated in *t.d.*, can be estimated. The thermal dose is a parameter utilized in safety engineering to evaluate the severity of burnings to the human skin. It can be determined from Equation (2.15), where q is the heat radiation in kW/m^2 and t is the fireball duration in s [43]:

$$t.d. = q^{4/3} \cdot t \tag{2.15}$$

As shown in Table 2.3, numerous thresholds have been proposed by various authors to discriminate the different burning injuries. These thresholds give a conservative reference when the heat radiation damages are analyzed since they consider the harm to the bare skin. For this reason, some reduction in the hazard distances might be made when the protection given by the presence of clothing is taken into account [43].

Table 2.3: Burns vs. thermal dose relationship.

Harm Caused	**Thermal Dose (kW/m^2)$^{4/3}$s**	
	Rew 1997 [44]	**O'Sullivan 2004** [45]
Pain threshold	-	92
Threshold 1° degree burn	80	105
Threshold 2° degree burn	240	290
Threshold 3° degree burn	1000	1000
50% Fatality	2000	2000

3 Case studies

Multiple tests have been performed with a range of different fuels, like propane or LNGT, to analyze BLEVEs and PVBs consequences to improve the safety of industrial facilities. In the last decades, the growing interest in hydrogen led to investigate also this relatively new fuel. Despite this, the number of tests is still limited. In this chapter, the experiments realized to investigate the explosion of hydrogen tanks, for both liquid and gaseous hydrogen, are presented. These tests will be the ones considered for the fireball analysis carried out in the next section of this thesis. In Table 3.1 the main experimental data obtained by the tests, besides NASA experiments, are summarized. NASA tests are considered separately because they investigate the explosion of tanks containing hydrogen propellant, that is a mixture of liquid hydrogen and liquid oxygen, and not only H_2.

Table 3.1: Hydrogen tank rupture experiments (excluded the NASA tests).

Experiment	**Type of explosion**	**Mass of fuel (kg)**	**Burst pressure (MPa)**	**Fireball diameter (m)**	**Fireball duration (s)**
BMW (1996) [46]	BLEVE	1.8-5.4	<1.29	20	4
SH2IFT (2021) [8]	BLEVE	27	5	25.8	5
Zalosh (2005) [47]	PVB	1.64	35.7	7.7	2
Zalosh (2007) [48]	PVB	1.87	34.5	24	2
Tamura (2006) - 1 [49]	PVB	1.406	99.47	18	2
Tamura (2006) - 2 [49]	PVB	1.367	94.54	18	2
Shen (2018) [50]	PVB	3.9	43.73	7-8	1.5

3.1 BLEVE tests

The number of BLEVE tests on hydrogen tanks is limited. Up to now, only two series of tests have been carried out on this kind of explosion:

- BMW tests, performed in the period 1992-1995, investigated the cold BLEVE consequences of small-scale hydrogen tanks for automotive application [46];
- SH2IFT tests, realized in the period 2018-2022, analyzed the hot BLEVE effects of three medium-scale liquid hydrogen storage vessels [8].

In the following two subsections, these experiments are presented in more detail.

3.1.1 BMW test series

BMW was the first company that investigated the consequences of BLEVE in small hydrogen tanks, with the aim of starting to use hydrogen combustion systems in the automotive sector. During a four-year research program, that lasted from 1992 to 1995, ten cold BLEVE experiments were performed. The vessels were single-wall tanks insulated with a layer of foam and a volume equivalent to the one of the inner vessel of liquid hydrogen vehicles (around 0.120m^3) [46]. All the tank tests were equipped with sensors to monitor the level, pressure, and temperature of the hydrogen content. The rupture of the vessels was performed in various conditions by means of cutting charges, that broke the tanks within a time interval of 0.2ms, as shown in Figure 3.1.

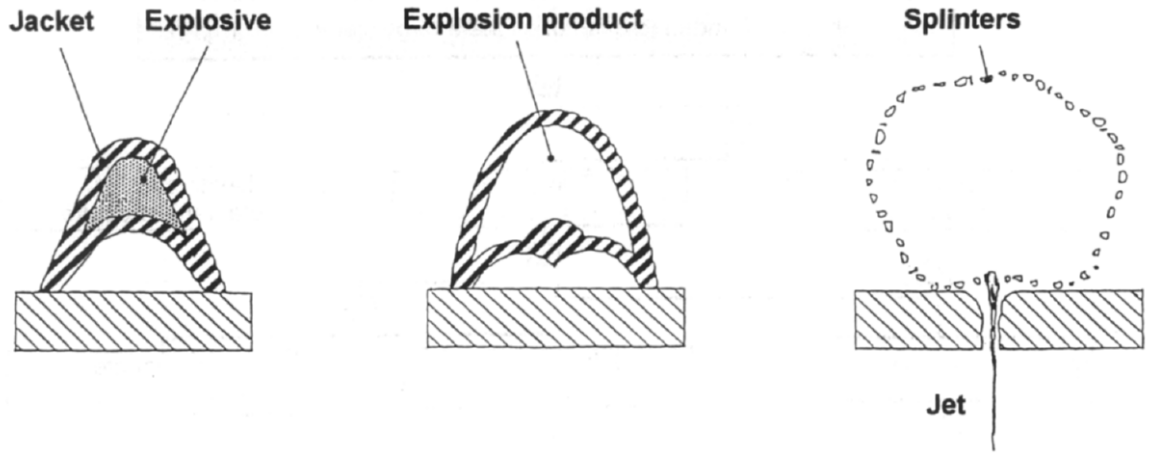

Figure 3.1: Jet development of a cutting charge [46].

The burst pressures were all below the critical pressure level of H_2 (1.29MPa), except one tank that ruptured at 1.48MPa. Every tank was filled with an amount of hydrogen that varied between 1.8 and 5.4kg and it was spontaneously ignited by the cutting jet generated from the exploding charges [46]. The fireballs generated by the rupture process reached a maximum diameter of 20m, lasting up to 4s. The fireballs started to lift off at the latest 1.8s after the ignition, reaching a maximum height between 16 and 20m [46]. All the data presented in the article and related to the fireball describe only the most severe consequences, without any correlation to the specific test and the hydrogen mass contained in the tank.

3.1.2 SH2IFT project

The *Safe Hydrogen Fuel Handling and Use for Efficient Implementation*, abbreviated in SH2IFT, was a project with the aim of "increase competence within safety of hydrogen technology, especially focussing on consequences of handling and use of large volumes and within closed and semi-closed environments and in maritime transport" [9]. This project lasted from 2018 to 2022, and during that period experiments on BLEVE were performed at the Test Site Technical Safety (TTS) of the Bundesanstalt für Materialforschung und–prüfung (BAM) in Horstwalde, Germany [8]. Three tests were performed varying some parameters, like the orientation of the vessel and the material used for the insulation. Of three tests, only one led to a BLEVE and, thus, it will be the only one described in the following.

The experiment has been carried out on a medium-scale $1m^3$ horizontal vessel, placed 1m above the ground. To minimize the heat dispersion, the tank was a double-walled vacuum-insulated vessel, with multi-layer insulation (MLI) as insulation material. The inner vessel had a thickness of 3mm, the outer vessel was 4mm and the heads were 5mm both. The material used for the vessels was a low-temperature resistant stainless steel (X5 CrNi 18-10), with a maximum allowable pressure of 0.9MPa. The filling degree was in the range 35% - 40%, leading to an LH_2 content of 27kg [8].

The test was performed by applying a heat load to the tank, provided by 36 propane burners. The safety valve was deactivated to force a pressure build-up and to increase the probability of tank failure. To monitor multiple parameters, such as temperature, pressure, and heat radiation, numerous sensors and equipment were implemented. At the time of the experiment, the relative humidity was 66.2% and the ambient temperature was 18.5°C [8].

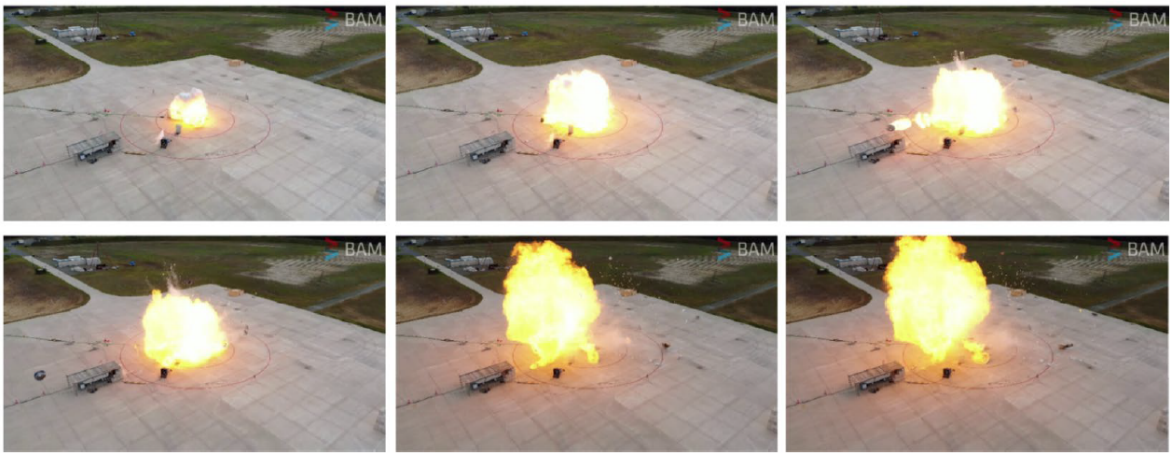

Figure 3.2: Evolution of fireball after the tank rupture of SH2IFT test [8].

After the beginning of the experiment, the pressure started to grow because of the hydrogen vaporization process induced by the heat load. The vessel, weakened by the

fire, started leaking approximately 40 minutes after the beginning of the test, leading to a stop in the increase of the internal pressure, which remained steady at about 5MPa. The tank failure resulted in a hydrogen BLEVE after around 1 hour, with consequent pressure waves generation, fragments, and a fireball, that is shown in Figure 3.2. At the time of failure, the temperatures of the gas and liquid phases were estimated to be -180°C for the former and -245°C for the latter. Because of the leakage, the mass of hydrogen at the time of failure is unknown [8].

Even if in [8] it is stated that the fireball reached a maximum diameter of 20m, more accurate measures, not published yet, conducted to a new estimation for the maximum diameter of 25.8m. The total duration of the fireball was about 5s, with the lift-off that started after 2s. Three bolometers were placed at 50m, 70m, and 90m from the center of the tank. Thanks to these instruments, the heat radiation was measured, reaching a maximum value of 2.1kW/m^2 at 70m and 1.2kW/m^2 at 90m. The sensor positioned at 50m reached saturation, due to an incident heat radiation that exceeded 2.4kW/m^2 [8].

3.2 Compressed hydrogen tests

The amount of data related to hydrogen PVBs is slightly higher compared to hydrogen BLEVEs. In the last two decades, five different experiments have been carried out, trying to obtain a better understanding of the consequences of CGH_2 storage tank failure. The experimental setups and the results related to the fireballs of these tests are now described.

3.2.1 Zalosh tests

Zalosh performed two tests on hydrogen PVBs in 2005 and 2007. In these tests, type IV and III tanks were used respectively. Both the vessels were lacking of a pressure relief valve (PRV), in order to ensure their failure [47, 48].

The first one was a 0.0724m^3 type IV tank filled with 1.64kg of hydrogen, with an initial pressure of 34.3MPa and an initial temperature of 27°C. It was a cylindrical vessel composed of three layers: an inner liner made of high-density polyethylene, a carbon fiber structural layer, and a protective fiberglass on the outside. It was exposed to a propane fire and ruptured after 6min 27s, at a pressure of 34.3MPa, generating a fireball with a diameter of 7.7m [47].

The other test was executed on a 0.088m^3 type III vessel, filled with 1.89kg of hydrogen [51]. This tank was placed under a Sport Utility Vehicle (SUV) and heated up through propane burners. The inner pressure remained constant at 31.8MPa, at least until 1min 24s when the pressure transducer stopped working, and failed after

12min 18s, generating a fireball of 24m of diameter [48].

The fireballs of both the two tests lasted around 2s, with the lift-off that occurred after about 1s [47, 48].

3.2.2 Tamura tests

In 2006, a couple of fire experiments were conducted in Japan by Tamura on two hydrogen tanks with a nominal working pressure of 70MPa. The first test involved a 0.036m^3 type III vessel, filled with 1.406kg of hydrogen [51], that ruptured at a pressure of 99.47MPa after 11min of fire exposure [49]. The second test was carried out on a 0.035m^3 type IV tank. It was filled with 1.367kg of hydrogen [51] and failed after 21min at the burst pressure of 94.54MPa. Both experiments generated fireballs of 18m in diameter, that lasted for around 2s [49].

3.2.3 Shen test

The test described by Shen was performed on a 0.165m^3 type III fully-wrapped carbon fiber reinforced composite tank with a 6061aluminum liner. The vessel was filled with compressed hydrogen gas at the nominal working pressure of 35MPa, thus achieving 3.9kg of fuel content. The tank failed after 17min 36s of fire exposure, at the burst pressure of 43.73MPa. The rupture was localized on a cup head, propelling the tank forward, as shown in Figure 3.3.

The generated fireball lasted for 1.5s and occupied the whole camera screen. For this reason, the fireball dimension was estimated between 7 and 8m, based on the size of the surrounding stones that were on site [50].

Figure 3.3: Flying tank of Shen test [50].

3.3 NASA tests

The first data related to hydrogen tank explosions were provided by NASA. In the 1960s, during the Saturn research program, NASA tested different propellants that could be used for rocket propulsion. During those tests, they analysed also the consequences, in terms of diameter and duration, of fireballs generated from the propellant storage tank failures.

Table 3.2: NASA fireball tests results, adapted from [52].

Mass of propellant (kg)	**F:O**	**Fireball diameter (m)**	**Fireball duration (s)**
90.718	1:5	9.45	2.57
90.718	1:5	15.24	2.75
90.718	1:5	21.34	2.62
90.718	1:5	18.29	2.75
90.718	1:5	14.63	-
90.718	1:5	20.73	0.57
90.718	1:5	18.29	2.01
90.718	1:5	12.80	1.49
90.718	1:5	15.24	0.99
90.718	1:5	6.71	0.5
1.361	1:0	5.49	-
45359	1:5	115.8	0.5
19.958	1:5	11.89	1.35
19.958	1:5	10.67	1.31
20.412	1:5	12.19	1.05
20.412	1:5	12.19	1.11
20.412	1:5	11.58	0.96
20.412	1:5	10.67	0.9
20.412	1:5	10.67	1.13
20.412	1:5	12.19	1.05
19.958	1:5	11.58	0.7
101.60	1:5	18.59	1.37
102.06	1:5	19.20	1.12
102.06	1:5	19.81	1.2
1065.9	1:0	64.01	2.6

Among the various propellants, also the mix LH_2/LOX, where LOX stands for liquid oxygen, was tested. A total of 25 experiments were performed with LH_2/LOX

as propellant, and the results can be seen in Table 3.2. The data present a significant scatter, probably due to the difficulty in defining in an unambiguous way the fireball dimensions and to the changes in the photographic techniques utilized. Almost all the tests were carried out with a fuel-to-oxidizer ratio (F:O) equal to 1:5.

Thanks to the results, they were able to conclude that the fireball diameters were essentially independent of the particular propellant combination utilized. Also, when LH_2 is used, it is always completely consumed [52].

4 Materials and methods

In Chapter 2, numerous models utilized in safety engineering to describe the fireball behavior have been introduced. In this chapter, the models adopted for the study carried out in this thesis will be presented together with the methodology, applied through the use of the MATLAB programming environment [53].

4.1 Fireball models

Thanks to the experimental data coming from the SH2IFT test, a detailed study of the fireball heat radiation has been carried out. For this analysis, the results of the common models used to evaluate the heat radiation and the thermal dose were compared to the results coming from a more realistic description of the fireball, considered dynamic.

As already mentioned, there are several analytical models, proposed in the literature, that attempt to predict the fireball characteristics. Comparisons between experimental data and analytical formulas have been made, considering both PVB and BLEVE tests, to find some models that can describe properly the diameter and duration of hydrogen fireballs. Then, some new models that might be more suitable to the description of a hydrogen fireball have been proposed.

One of the main issues found during the study was related to the hydrogen mass of the BLEVE tests. Indeed, as stated in Chapter 3, the mass of hydrogen involved in BMW and SH2IFT experiments are uncertain. For the BMW tests the available data concern the most severe consequences in terms of diameter and duration and the range of H_2 masses the experiments were carried out with (1.8-5.4kg) [46]. Differently, in the SH2IFT test a hydrogen leakage occurred and, thus, the H_2 mass at the time of the explosion is unknown [8].

For this reason, an esteem of the lowest hydrogen mass content at the moment of the BLEVE in the SH2IFT test was achieved. To obtain a more conservative estimation, all the tank content has been considered to be in its gaseous phase and, then, the ideal gas law has been applied [54]:

$$PV = nRT \tag{4.1}$$

where P is the inner tank pressure, V is the internal tank volume, n is the hydrogen

number of moles, R is the ideal gas constant (8.314J/(mol· K) [54]) and T is the gas temperature at the moment of explosion. All the experimental data have been introduced in Chapter 3.

Since the only unknown term is n, the Equation (4.1) can be rewritten as:

$$n = \frac{P \cdot V}{R \cdot T} \tag{4.2}$$

Once the moles are calculated, the hydrogen mass can be determined by multiplying n with the molar mass M_m (2.016g/mol [54]):

$$m_f = n \cdot M_m \tag{4.3}$$

Following this calculation process, a lower limit of 13kg has been obtained. A similar estimation was also obtained using the CoolProp package [55].

This value is the one that will be mostly considered in the analysis, that will be discussed in Chapter 5 because allows more conservative results. At the same time, for the BMW tests a mass of 5.4kg is considered in the study because the major consequences are expected to happen with the higher values of masses.

4.1.1 Heat radiation

The analysis of the heat radiation of the SH2IFT test started from the data obtained by the three bolometers placed at 50m, 70m, and 90m from the tank center. These data cover a time span of almost 11s, that is more than the fireball duration observed. As already explained in Chapter 3, the sensor at 50m reached saturation during the fireball development. For this reason, a reconstruction of the heat radiation curve at 50m was performed.

First of all, the fireball SEP was calculated starting from the experimental data, thanks to Equation (2.5):

$$\text{SEP} = \frac{q}{F \cdot \tau_a} \tag{4.4}$$

where q is the heat radiation in kW/m^2. The equations presented in Section 2.4.2 were used to calculate the view factor F (Equation (2.9)) and the atmospheric transmissivity τ_a (Equations (2.10) to (2.12)). In particular, Equation (2.11) was used to calculate τ_a, as in [41].

The view factor was considered both steady and dynamic over time. In the first case, the fireball was deemed to be at its maximum height, chosen equal to the maximum diameter, for its whole duration. In the second case, also the lift-off was taken into account. To do so, the average lift-off velocity $v = \Delta x/\Delta t$ was calculated in three different ways, depending on the moment considered:

1) For the first 2s (time before lift-off), $\Delta x = \textit{Fireball radius} - \textit{Initial tank height}$;

2) For the next 3s, $\Delta x = \textit{Maximum fireball height} - \textit{Fireball radius}$;

3) For the last 6s of radiation, the fireball was considered steady at its maximum height.

The fireball diameter was always considered equal to the peak value (25.8m) for both cases.

To recreate the heat radiation curve at 50m, a SEP value had to be assumed. Two different SEP estimations have been adopted: *(I)* the average between the SEPs calculated at 70m and 90m, that will be addressed as *SEP avg*; *(II)* assuming the differences of the SEP values between 50m and 70m to be the same as between 70m and 90m. In this case, named *SEP fit*, the average SEP coincides with the one calculated at 70m.

Then, the heat radiation at 50m was calculated for all four cases:

- *SEP avg*, steady F;
- *SEP fit*, steady F;
- *SEP avg*, dynamic F;
- *SEP fit*, dynamic F.

Also, the maximum value of the average SEP was used to estimate the combustion temperature through the Stefan-Boltzmann law (Equation (2.6)) and compared to the temperature measured from the instruments employed during the experiment.

Finally, an estimation of the possible range for maximum SEP values was made by means of Equation (2.7), considering the lower and upper limits of hydrogen content (13-27kg).

4.1.2 Thermal dose and thermal hazard

After the reconstruction of the heat radiation curve at 50m, the study proceeded with the calculation of the thermal dose. Firstly, its trend during time was determined at 50m, 70m, and 90m, both for the steady and the dynamic cases. The *t.d.* was calculated as an integral during time through Equation (2.15), with $\Delta t = 0.005$s, that is the time interval between two different experimental data.

Then, the *t.d.* reached after the fireball extinction was calculated as a function of space, still for both the steady and dynamic cases. It was compared to the analytical thermal dose, that was calculated through Equation (2.15), with q equal to the peak heat radiation and $t = 5$s.

Also, the *t.d.* as a function of space and time was determined in the case "*SEP fit*, dynamic F".

Finally, the thermal hazard has been assessed and some hazardous distances have been calculated. The thresholds proposed by Rew [44], presented in Section 2.4.2 and here shown again in Table 4.1, have been chosen because they allow a more conservative evaluation.

The two MATLAB scripts created to perform the analysis of the heat radiation, the thermal dose, and the thermal hazard can be found in Appendices B and C.

Table 4.1: Burns vs. thermal dose relationship [44].

Harm Caused	**Thermal Dose $(kW/m^2)^{4/3}s$**
Threshold 1° degree burn	80
Threshold 2° degree burn	240
Threshold 3° degree burn	1000
50% Fatality	2000

4.1.3 Fireball dimension and duration

It is not easy to find an empirical correlation that can predict sufficiently well the fireball dimension and duration because of the complexity of the combustion process and the limited number of experiments. For this reason, before proposing some new models, a preliminary analysis with the analytical formulas found in the literature was made, both for the dimension and the duration of the fireball.

Fireball dimension

The empirical equations selected from the literature are also the ones analyzed by Makarov in [51]. First of all, the Roberts equation was chosen since it is the most used in safety engineering [39]. This formula has been already presented in Chapter 2 and it is here reported again:

$$D = 5.8 \cdot m_f^{1/3} \tag{4.5}$$

Another correlation is similar to the one proposed by Hord for hydrogen rocket propellants, and provides a larger diameter for the fireball [51]:

$$D = 7.93 \cdot m_f^{1/3} \tag{4.6}$$

Both these equations calculate the fireball diameter considering it as spherical. However, the fireball often assumes a different shape and, when it is not flattened, it acquires a hemispherical form, resulting in a diameter that is about $\sqrt[3]{2} \approx 1.26$ bigger [51]. For

this reason, another equation, that will be addressed as *Makarov hms.*, was proposed by Makarov [51]:

$$D = 9.8 \cdot m_f^{1/3} \tag{4.7}$$

Finally, another formula, that will be referred to as *Makarov cons.* was analyzed, still proposed by Makarov [51]. It fits the "worst-case scenario" among all the tests considered, i.e., the experiment made by Zalosh in 2007 [48]:

$$D = 19.5 \cdot m_f^{1/3} \tag{4.8}$$

Following this first comparison, other two equations were proposed. These correlations fit the data coming from BMW tests and from the SH2IFT experiment, considering the hydrogen mass content respectively equal to 5.4kg and 13kg for the reasons explained above. These equations are here presented:

$$D = 11.40 \cdot m_f^{1/3} \ \textit{(BMW fit)} \tag{4.9}$$

$$D = 10.97 \cdot m_f^{1/3} \ \textit{(SH2IFT fit)} \tag{4.10}$$

After this first analysis, another method to calculate the diameter, referred to as *I.G. EoS method*, has been adopted, based on the ideal gas law. Indeed, after the explosion, the pressure of hydrogen drops to the ambient pressure and the temperature increases because of the combustion. These conditions of low pressure and high temperature allow the gasses involved in the combustion process to be considered as ideal gasses [54].

To calculate the volume and, then, the diameter, Equation (4.1) can be rewritten as:

$$V = \frac{n \cdot R \cdot T}{P} \tag{4.11}$$

where n can be easily calculated from Equation (4.3) knowing the hydrogen mass. After the explosion, the fireball develops at ambient pressure. For this reason, P is considered equal to 0.1MPa.

The only parameter left to calculate the volume is T, which is assumed in this case the adiabatic flame temperature (T_{ad}). To estimate it, a method similar to the one presented in [56] was followed.

The first law of thermodynamics can be written as:

$$dQ = dH - VdP \tag{4.12}$$

Considering an isobaric and adiabatic combustion it becomes:

$$dQ = dH = 0 \tag{4.13}$$

Since enthalpy is a state function, Equation (4.13) can be rewritten as:

$$\Delta H = \sum_{i=1}^{N} a_i^{''} H_i(T_{ad}) - \sum_{i=1}^{N} a_i^{'} H_i(T_j) = 0 \tag{4.14}$$

and then,

$$\sum_{i=1}^{N} a_i^{''} \left[\Delta H_{f,i}^0 + \Delta H_i(T_{ad}) - \Delta H_i(T_{amb})\right] - \sum_{i=1}^{N} a_i^{'} \left[\Delta H_{f,i}^0 + \Delta H_i(T_j) - \Delta H_i(T_{amb})\right] \tag{4.15}$$

where:

a_i'' are the stoichiometric coefficients of the chemical products of the reaction;

a_i' are the stoichiometric coefficients of the chemical reactants of the reaction;

$\Delta H_{f,i}^0$ is the standard molar heat of formation of species i at P=0.1MPa and $T = T_{amb}$;

$\Delta H_i(T) = H_i(T) - H_i(0)$;

T_{ad} is the adiabatic flame temperature;

T_{amb} is the ambient temperature, equal to 298.15K;

T_j is the initial temperature of the reactants [56].

If the starting temperature of the reactants is $T_j = T_{amb}$ and their enthalpy of formation is equal to 0, Equation (4.15) can be simplified in this way:

$$\sum_{i=1}^{N} a_i^{''} \left[\Delta H_{f,i}^0 + \Delta H_i(T_{ad}) - \Delta H_i(T_{amb})\right] = 0 \tag{4.16}$$

The combustion reaction of hydrogen in air is:

$$H_2 + \frac{1}{2}O_2 + \frac{79}{42}N_2 \rightarrow H_2O + \frac{79}{42}N_2 \tag{4.17}$$

The only chemical compound that has an enthalpy of formation different from 0 is H_2O ($\Delta H_{f,H_2O}^0 = -241.818$kJ/mol [57]).

Since the gasses are considered as ideal, $\Delta H(T) = c_p(T) \cdot \Delta T$ and, then, Equation (4.16) can be modified in:

$$-\Delta H_{f,H_2O}^0 = \sum_{i=1}^{N} a_i^{''} c_{p,i}(T_{avg}) \cdot [T_{ad} - T_{amb}] \tag{4.18}$$

where $T_{avg} = 0.5 \cdot (T_{ad} - T_{amb})$. Finally, replacing $\sum_{i=1}^{N} a_i'' c_{p,i}(T_{avg})$ with $c_{p,avg}(T_{avg})$, Equation (4.19) can be obtained:

$$-\Delta H^0_{f,H_2O} = c_{p,avg}(T_{avg}) \cdot [T_{ad} - T_{amb}] \tag{4.19}$$

From Equation (4.19), an iterative calculation has been adopted to find T_{ad}, following these steps:

1) A first attempt T_{avg} is assumed;

2) The $c_{p,i}(T_{avg})$ are determined by interpolation from the table in Appendix A;

3) $c_{p,avg}(T_{avg})$ is calculated;

4) T_{ad} is determined from Equation (4.19);

5) T_{avg} is calculated again and compared with the one assumed in the first step. If their difference is within a certain range, the T_{ad} determined in step 4 is the correct one, otherwise, another iteration is needed, starting again from step 1.

Once the adiabatic flame temperature is calculated (in this case it is equal to 2487K), the volume of hydrogen at T_{ad} can be determined with Equation (4.11). That volume has to be divided by 0.3, that is the stoichiometric H_2/air mixture ratio [5], to take into account the air entrainment. Actually, the H_2/air mixture ratio changes during the combustion process. However, trying to indicate an average burning condition, it was believed reasonable to consider the mixture to be stoichiometric.

In the end, when this new volume is calculated, also the diameter of the fireball, considered as a sphere, can be determined:

$$d = 2 \cdot \sqrt[3]{\frac{3}{4\pi} V} \tag{4.20}$$

This method was applied to all the tests considered in this thesis using Microsoft Excel [58] and a new empirical formula, named *I.G. EoS fit*, based on its results was proposed:

$$D = 12.74 \cdot m_f^{1/3} \tag{4.21}$$

Fireball duration

Only two equations were selected from the literature to analyze the fireball duration. They are the ones proposed by CCPS for momentum-driven and buoyancy-driven fireballs [29]. They are respectively:

$$t = 0.45 \cdot m_f^{1/3} \tag{4.22}$$

$$t = 2.6 \cdot m_f^{1/6} \tag{4.23}$$

Then, other formulas that fit the data from the SH2IFT experiment have been tested. They are named *Momentum-driven Fit* (Equation (4.24)), *Buoyancy-driven Fit* (Equation (4.25)) and *BMW-SH2IFT Fit* (Equation (4.26)):

$$t = 2.13 \cdot m_f^{1/3} \tag{4.24}$$

$$t = 3.26 \cdot m_f^{1/6} \tag{4.25}$$

$$t = 2.61 \cdot m_f^{1/4} \tag{4.26}$$

Also, other three equations, based on the momentum-driven phenomenon, were proposed to indicate an optimal correlation that can better describe all the experimental data. To do so, the data from Shen experiment [50] has been ignored, since it represents an isolated point. The *optimal fit* equation resulted to be:

$$t = 1.96 \cdot m_f^{1/3} \tag{4.27}$$

while other two relations determine the upper limit (Equation (4.28)) and the lower limit (Equation (4.29)) identified for fireball duration:

$$t = 2.28 \cdot m_f^{1/3} \tag{4.28}$$

$$t = 1.60 \cdot m_f^{1/3} \tag{4.29}$$

Finally, for both the dimension and the duration, the relative errors of the different models, in percentage, were calculated through Equation (4.30):

$$Relative\ error = 100 \cdot \frac{Model\ estimation - Experimental\ data}{Experimental\ data} \tag{4.30}$$

5 Results and discussion

In this last chapter, the results of the analysis presented in Chapter 4 are shown. The outcomes are discussed in a comparative way in the following tables and graphs, generated with MATLAB [53], making a comparison between how the different models describe the fireball characteristics.

In the first part of the chapter, the study of the heat radiation and the thermal hazard of the fireball from the SH2IFT project is carried out. Then, the results of the different models selected and proposed to predict the fireball dimension and duration are presented. Finally, the diameters and durations of the tests from NASA are analyzed and the models that are more suitable for their description are shown.

5.1 SH2IFT project

The SH2IFT project provided data related to the heat radiation coming from the fireball, along with the ones about its diameter and duration. Therefore, the fireball-measured thermal hazard was studied and compared to the one calculated with the analytical models found in the literature.

Before analyzing the thermal dose, a fitting of the experimental data, missing because of the instrument saturation, was tried. Also, the combustion temperature was calculated through Stefan-Boltzmann's law (Equation (2.6)) and compared to the one measured from the thermal cameras.

5.1.1 Fireball surface emissive power

The data concerning the incident radiation, collected by the bolometers, are reported in Figure 5.1. The instrument placed at 50m from the tank center was in overload for around 3s and, thus, the heat radiation measurement stopped at its maximum scope, which was 2.4kW/m^2. For this reason, before proceeding with the analysis of the thermal hazard, a reconstruction of the heat radiation curve at 50m was tried, starting from the SEP calculation.

Equation (2.7) gives us a first estimation of the possible range of the SEP values. Considering the SH2IFT BLEVE, the equation can be solved with the following

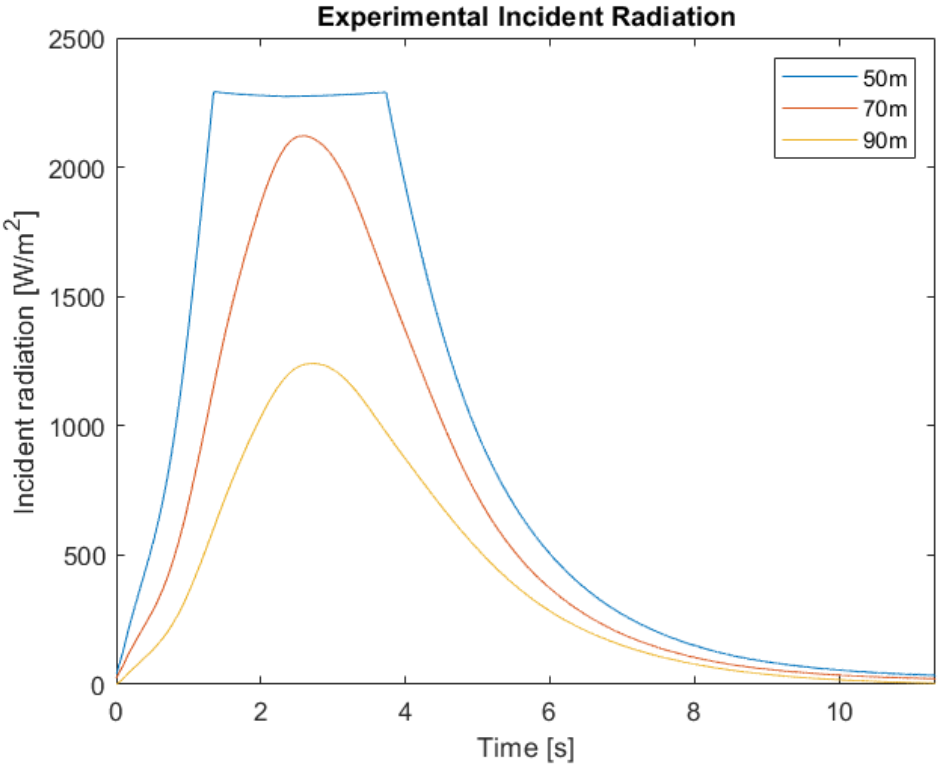

Figure 5.1: Experimental incident radiation (adapted from [8]).

parameters:

- P = $5 \cdot 10^6$Pa [8];
- ΔH_c = 118.8MJ/kg [59];
- D = 25.8m;
- t = 5s [8];
- m_f = 13-27kg.

By imposing the upper and the lower limits for the hydrogen mass, identified in Chapter 4 and equal to the values of m_f indicated above, the SEP estimation varies between 66.83kW/m^2 and 138.80kW/m^2.

Then, the actual SEP variation during time was calculated from the experimental incident radiation data through Equation (4.4). The results were used to identify a surface emissive power that could better fit the data coming from the bolometer at 50m, considering the view factor F both steady and dynamic. As already explained in Chapter 4, two different SEP estimations were achieved: *SEP avg* and *SEP fit*. Figures 5.2 and 5.3 show the surface emissive power variation for the cases with steady and dynamic F.

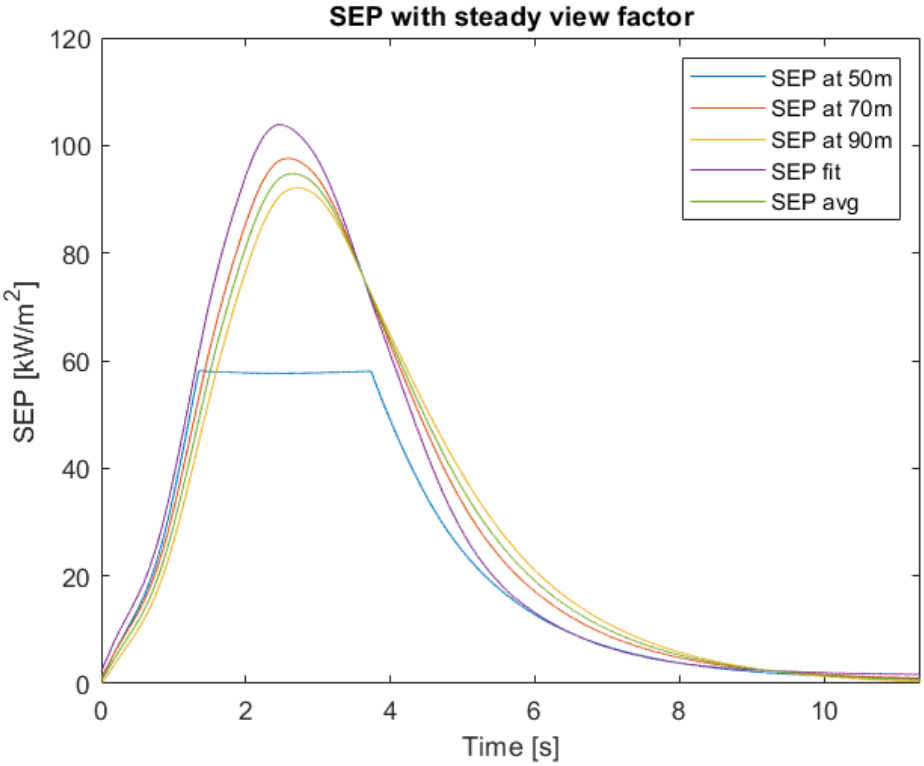

Figure 5.2: SEP variation during time, with steady view factor.

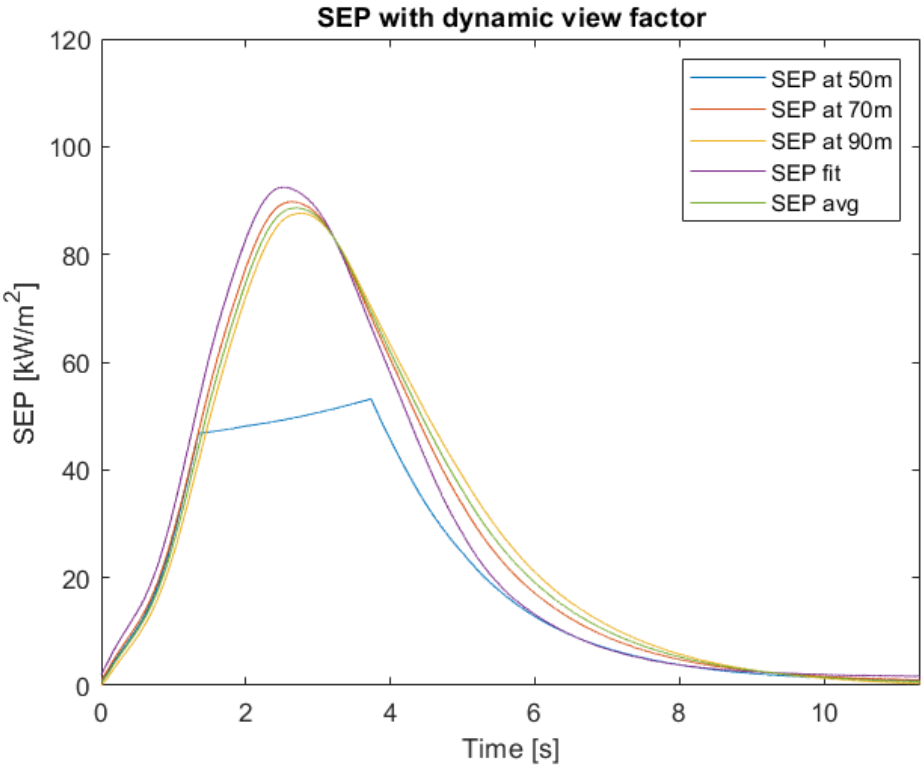

Figure 5.3: SEP variation during time, with dynamic view factor.

In both cases, the *SEP fit* seems to better describe the real trend of the surface emissive power at 50m. In particular, the violet line follows very well the blue one at the beginning of the fireball development, with only a little overestimation in the "dynamic F" case, and they become coincident around 6s after the start of the BLEVE event. Meanwhile, the *SEP avg* describes well the experimental data during the first two seconds, but it overestimates them during almost all the descending phase of the curve, with the green line that reaches the blue one only at 9s. However, both the surface emissive powers have been initially used for the estimation of the thermal dose, that will be presented in the following (Section 5.1.3).

Another noteworthy aspect of Figures 5.2 and 5.3 is that a steady view factor brings to higher SEP values. Indeed, the peak that the surface emissive power reaches at 70m is 97.62kW/m^2 with the steady F, and 89.77kW/m^2 considering F as dynamic. This fact does not directly imply that the thermal hazard will be worse considering a steady F. Indeed, the heat radiation depends not only on the SEP, but also on the view factor and on the atmospheric transmissivity, as can be seen in Equation (2.5). Thus, if also these last two parameters are considered to change with time, the incident radiation stops to be directly proportional to the surface emissive power and its behavior becomes more complex.

It has to be noted that the maximum SEP values just mentioned are in the range calculated above, suggesting that Equation (2.7) might be reliable also for the hydrogen fireball SEP estimation.

Finally, from these maximum values, an estimation of the average combustion temperature was obtained through Equation (2.6), resulting in a flame temperature of almost 1150K. This temperature is lower than the one measured from the thermal camera during the experiment, which was around 1650K. This aspect can be explained by considering that the thermal camera measures the maximum temperature reached by the flame, while the estimation gives us an average value of the combustion temperature.

5.1.2 Heat radiation

With the SEP values presented above, the heat radiation has been calculated again trough Equation (2.5), obtaining four different incident radiation estimations at 50m, as Figures 5.4 and 5.5 show. Clearly, the heat radiations at 70m and 90m remained the same as the experimental data.

Figure 5.4 also shows that the experimental data of the heat radiation at 50m are better described with the estimation made considering the *SEP fit*. Indeed, the violet line is almost coincident with the blue one in the first part of the graph, and they become coincident around 6s after the beginning of the data. Differently, the estimation

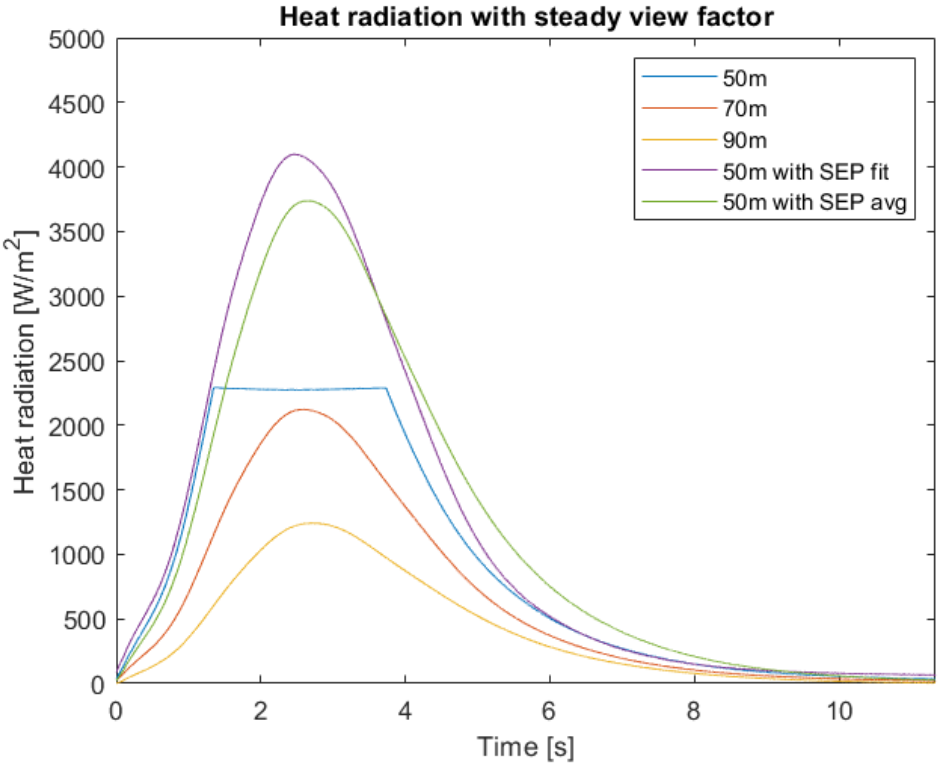

Figure 5.4: Heat radiation estimation during time, with steady view factor.

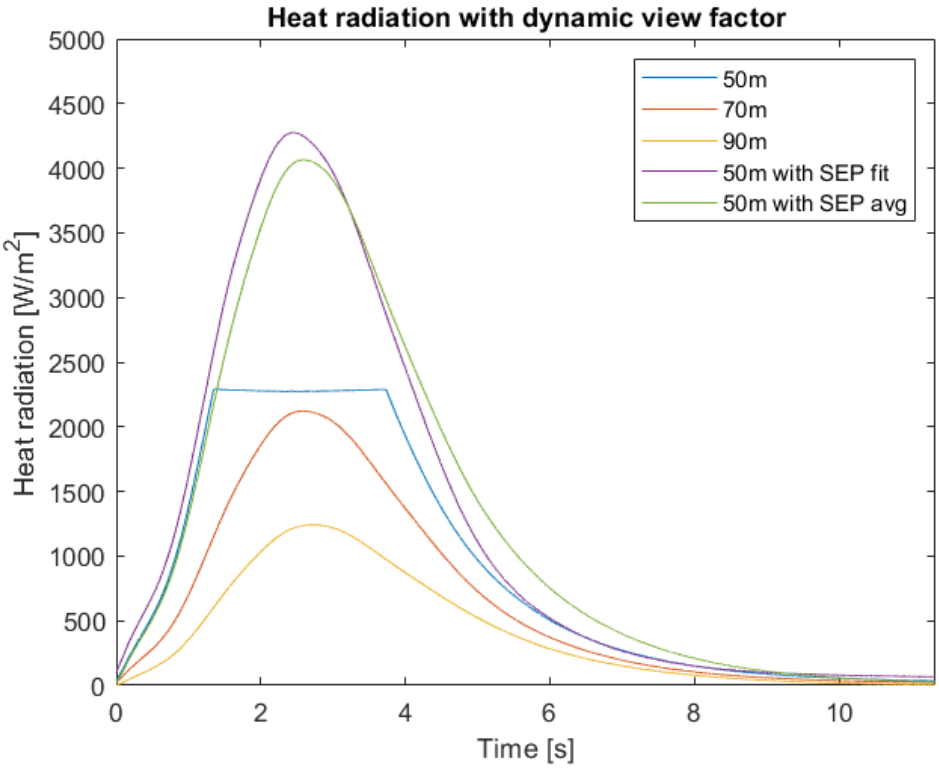

Figure 5.5: Heat radiation estimation during time, with dynamic view factor.

made considering the *SEP avg* brings to a little underestimation of the heat radiation in the first 1.5s, while it overestimates the curve for almost all its descending part. These trends are the same as the ones observed in Figure 5.2 for the SEP estimation since steady values of F and τ_a make the surface emissive power and the heat radiation directly proportional.

A similar trend can be noticed in Figure 5.5, with both the green and the violet lines that overestimate the experimental data in the descending part of the curve, but with the heat radiation calculated with *SEP fit* that becomes coincident with the measures (blue line) before the other, resulting in a more precise estimation.

The main differences between Figure 5.4 and Figure 5.5 are in the first part of the chart, where the heat radiation starts to grow up, and in the maximum radiation values calculated at 50m. Indeed, in the first 1.5s, the estimation obtained with *SEP avg* is more accurate compared to the other evaluation made, that slightly overestimates the experimental data. Also, the heat radiation calculated at 50m is greater considering the view factor as dynamic, with a peak of 4278W/m^2 versus 4099W/m^2, even if the maximum surface emissive power was lower in this case. The explanation of this difference has been already discussed in Section 5.1.1.

5.1.3 Thermal dose and safety distances

After the SEP and the heat radiation curves fitting, the analysis proceeded with the thermal dose calculation. First of all, the *t.d.* has been calculated as a function of time for the three distances where the bolometers were placed. For the radiation at 50m, both the estimations presented before have been examined. Figures 5.6 and 5.7 show the results.

The thermal dose reaches similar values in both cases and, at the distances considered, remains far below the safety threshold of $80(\text{kW/m}^2)^{4/3}$s, even considering the "worst case scenario", in which a person gets all the radiation coming from the fireball. Also, despite the differences that have been shown about the heat radiation estimations at 50m, when considering the thermal dose, both the cases bring to a similar result, that is around $20(\text{kW/m}^2)^{4/3}$s. Still, the *t.d.* calculated considering the *SEP fit* is slightly more conservative and, for this reason, it is the one selected for the analysis that will be presented in the following (Figures 5.8 and 5.9).

Another interesting aspect to be noted is that 95% of the total thermal dose is released in the first 5.26s. Therefore, the thermal dose received from any target is equal to the final values reported in the graphs, given the short reaction time.

Moreover, the space-dependency of the thermal dose has been considered, to obtain some more useful information for the safety investigation. In this case, the experimental data, equal to the final values of the previous analysis, were compared to the results

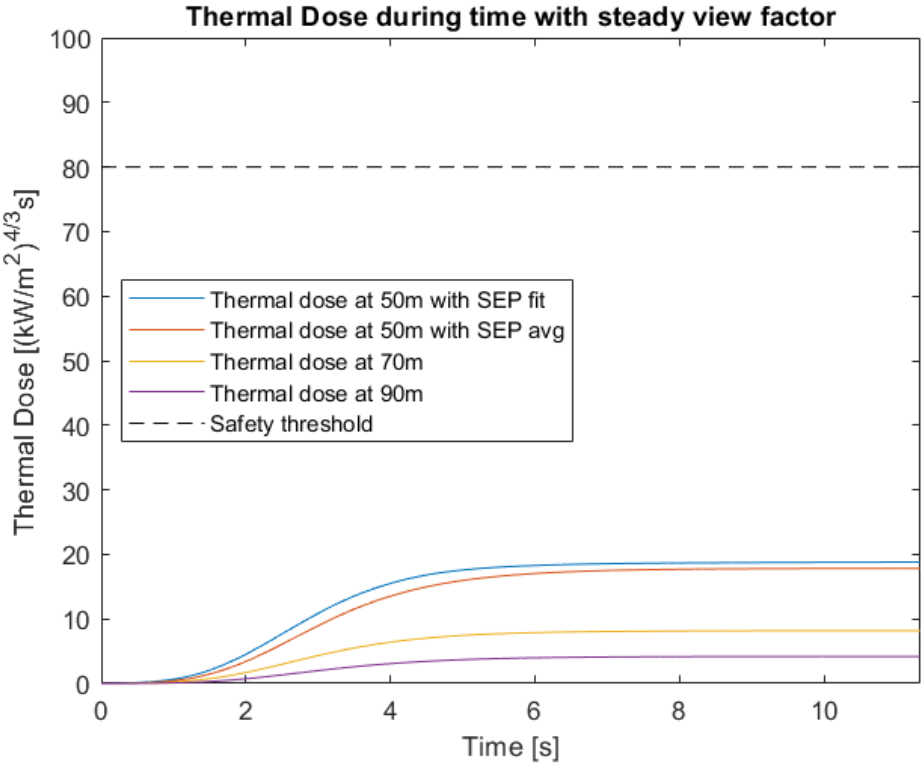

Figure 5.6: Thermal dose as a function of time, with steady view factor.

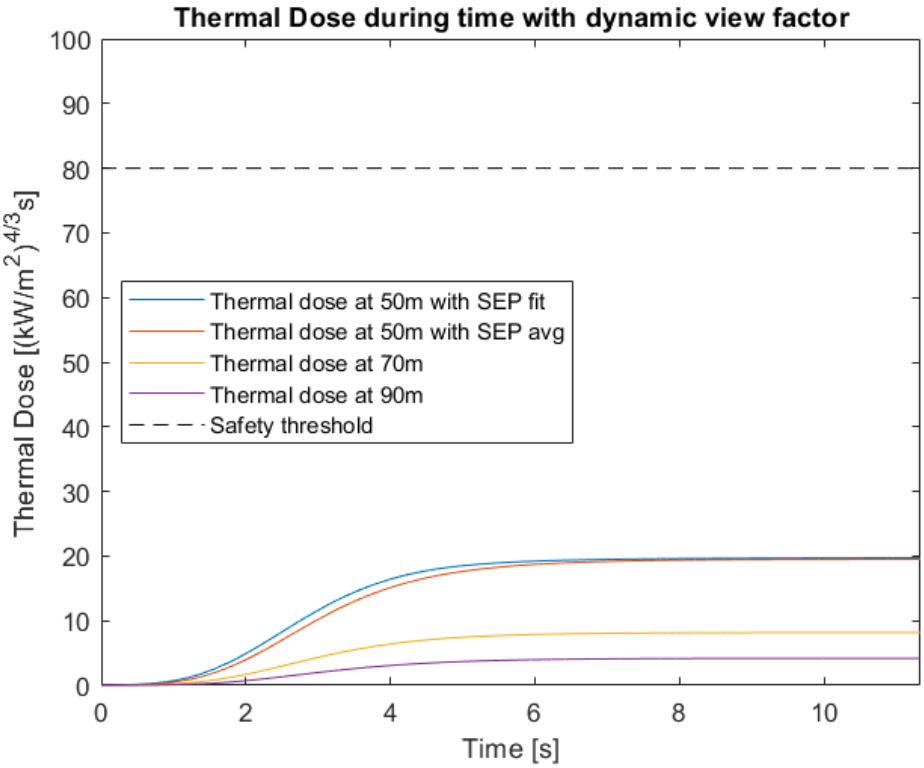

Figure 5.7: Thermal dose as a function of time, with dynamic view factor.

obtained with Equation (2.15), where q is again calculated through Equation (2.5).

Since the fireball is characterized by only one value of surface emissive power, that does not change with the distance the heat radiation is measured from, an average has been selected to estimate the thermal hazard. This average coincides with the SEP calculated at 70m, since the *SEP fit* was selected for the radiation at 50m, and its maximum value has been chosen to perform the computation.

An average SEP has been calculated even to fit the experimental data, obtaining values of 66.70kW/m^2 and 67.55kW/m^2 respectively for the cases with a steady and a dynamic view factor. Then, Figures 5.8 and 5.9 have been obtained.

The following charts explain that the maximum thermal dose reached next to the fireball is almost the same considering both F as steady and dynamic. Furthermore, the analytical estimation is more conservative in either case, when compared to the experimental data, and it reaches higher values with a steady view factor, since the correlated SEP is greater.

Table 5.1: Calculated hazardous distances with steady view factor.

Harm Caused	**Distance from fireball center (m)**	
	Experimental	**Analytical**
No harm	>22	>31
1° degree burn	12.9-22	12.9-31
2° degree burn	<12.9	<12.9
3° degree burn	<12.9	<12.9
50% Fatality	<12.9	<12.9

Table 5.2: Calculated hazardous distances with dynamic view factor.

Harm Caused	**Distance from fireball center (m)**	
	Experimental	**Analytical**
No harm	>22	>29
1° degree burn	12.9-22	12.9-29
2° degree burn	<12.9	<12.9
3° degree burn	<12.9	<12.9
50% Fatality	<12.9	<12.9

To get a more clear representation of the thermal hazard correlated to the SH2IFT project fireball, the safety distances have been calculated, considering the thresholds presented in Chapter 4, and are reported in Tables 5.1 and 5.2.

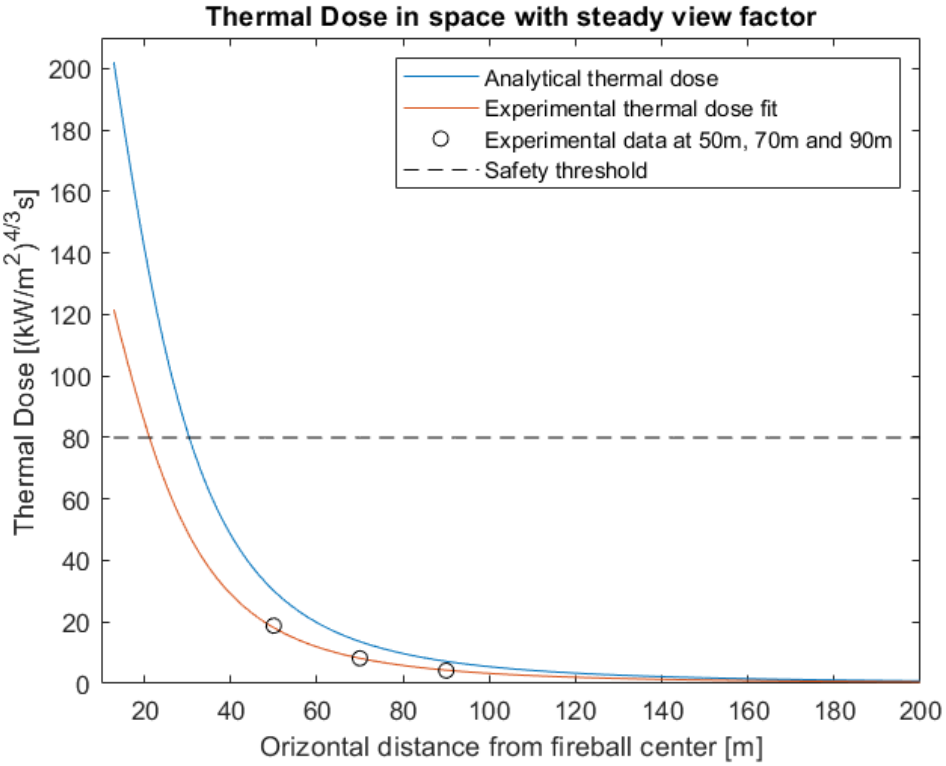

Figure 5.8: Thermal dose as a function of time, with steady view factor.

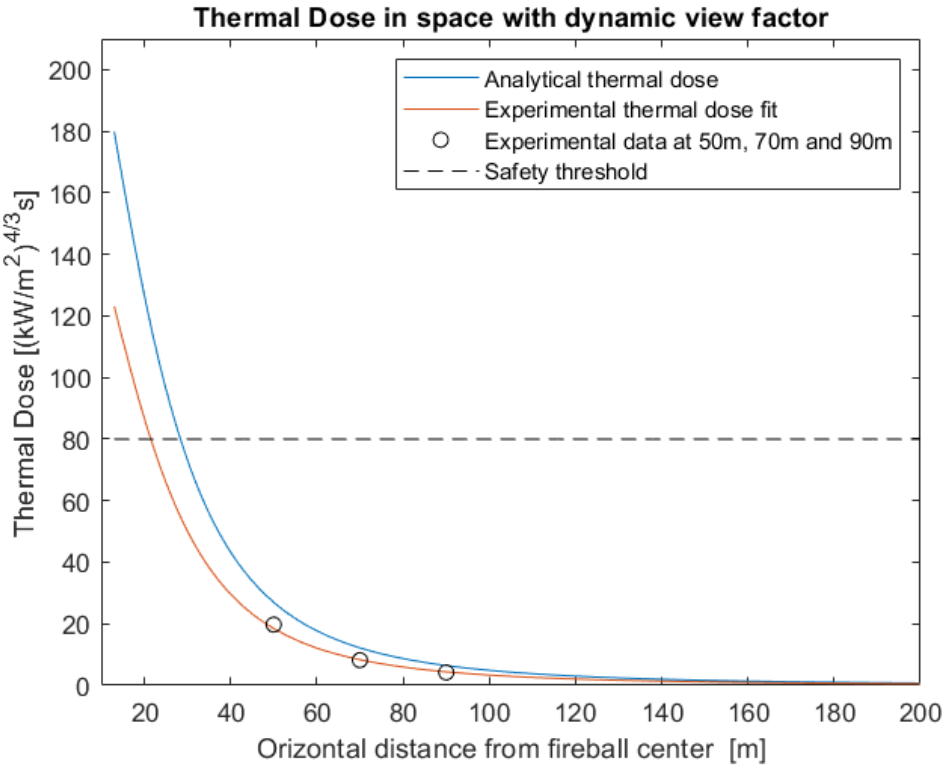

Figure 5.9: Thermal dose as a function of time, with dynamic view factor.

The thermal hazard is different from zero only in the proximity of the fireball and it is limited to 1° degree burns up to 22m. Since the fireball radius is about 12.9m, it means that no injuries are expected at a distance greater than 10m from the fireball limits. Furthermore, the safety distances calculated have been obtained considering the most conservative thresholds found in literature, referred to the bare skin. Thus, the actual hazard ranges might be lower if the real conditions are taken into account, such as the use of fireproof clothes by the workers. Still, if a person is found in the range reached by the fireball at the moment of the BLEVE accident, the consequences can become very severe, with a high probability of fatality.

Finally, Figure 5.10 depicts how the thermal dose evolves in space and during time. Again, it shows a strong time-dependency, giving no time to escape to any people involved, and it decreases with the distance, leading to minor consequences if the people are out of range of the fireball.

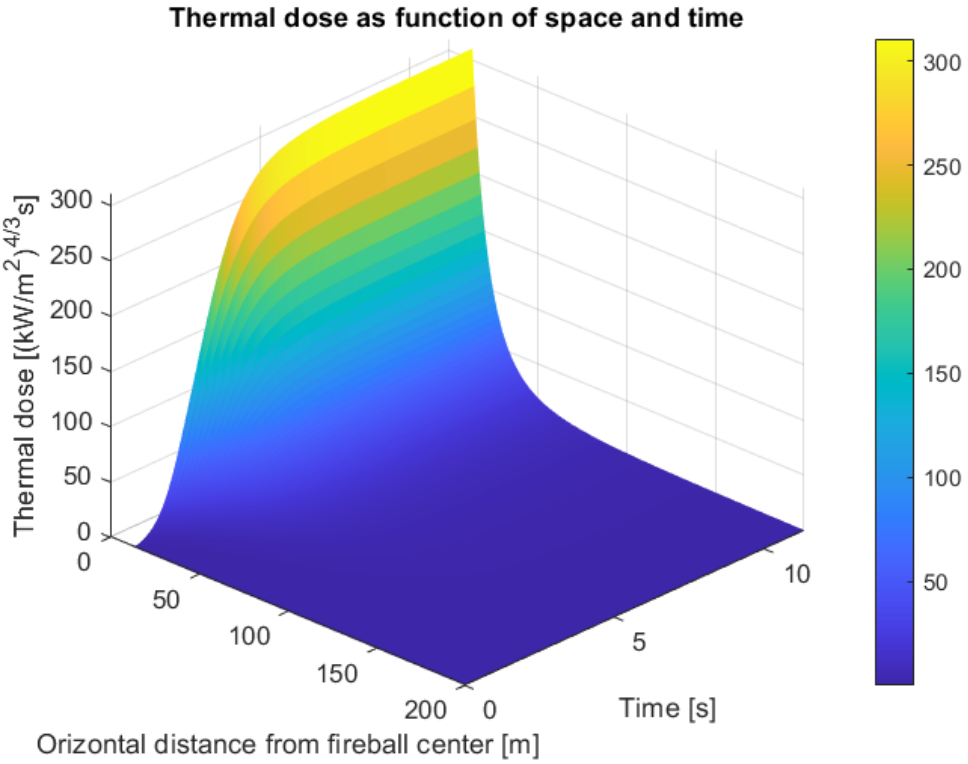

Figure 5.10: Thermal dose as a function of space and time.

5.2 PVBs and BLEVEs prediction models

As seen in Section 4.1.1, the knowledge of the diameter and the duration of the fireball is crucial to predict the fireball thermal hazard. These parameters can be obtained by

means of different models, experimental evidence, analytical formulas, or by Computational Fluid Dynamics (CFD) simulations. In this section, the analytic models selected from the literature and the new ones proposed to describe the fireball dimension and duration are compared using experimental data, coming from both the PVB and the BLEVE hydrogen tests presented in Chapter 3.

5.2.1 Fireball diameter

The analysis of the fireball diameter started with the models proposed by Makarov [51] and introduced in Chapter 4. In this case, the data of hydrogen BLEVEs coming from the BMW test series and the SH2IFT project are considered, along with the PVB data. Figure 5.11 shows this comparison.

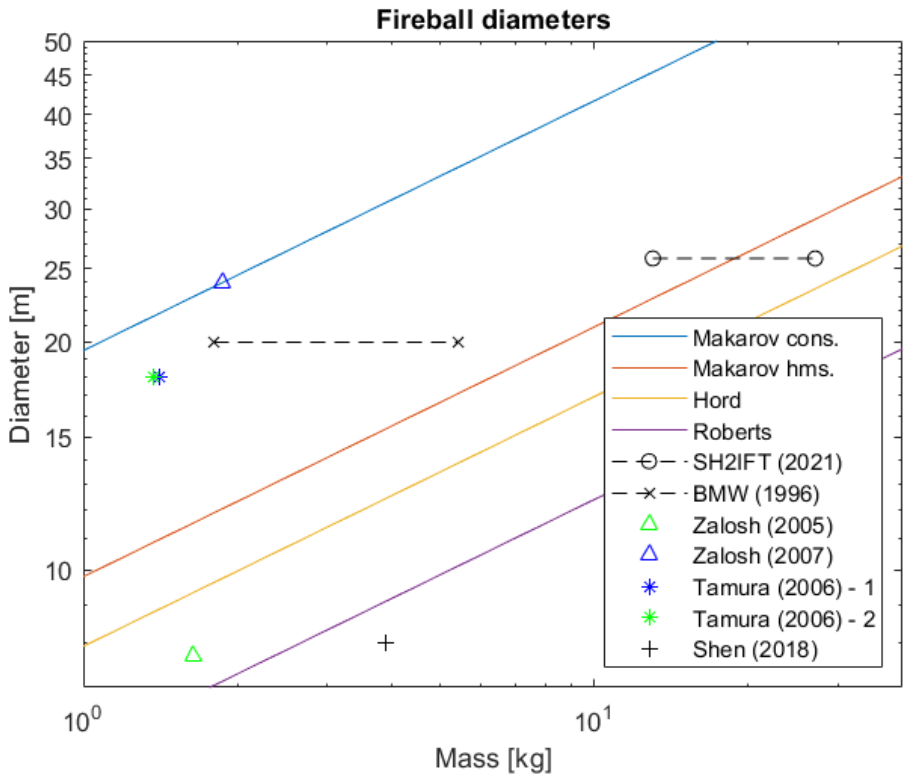

Figure 5.11: Diameter: models from the literature vs experimental data.

Noteworthy is that the Roberts equation, which works well for the majority of the fuels, is not able to describe properly the hydrogen fireballs, since it generally underestimates them. Only the data from Zalosh (2005) and Shen (2018) seem to verify the reliability of the Roberts equation, which, of course, does not provide statistical relevance. Furthermore, the latter experienced a particular tank rupture [50] and, thus, it is speculated that the dimension is atypically small.

The Hord and the *Makarov hms.* models also underestimate the fireball diameters.

However, in this case, the estimations are closer to the experimental data, with the *Makarov hms.* model that describes quite well the data from the BLEVE experiments.

Both the data from Tamura (2006) and the one from Zalosh (2007) display very large fireballs with small hydrogen masses. This is due to the fact that the fireballs were flattened and, thus, their shapes were neither spherical nor hemispherical [51]. The *Makarov cons.* equation was proposed to fit the Zalosh (2007) data and continue to be the most conservative model, since it overestimates all the experimental data.

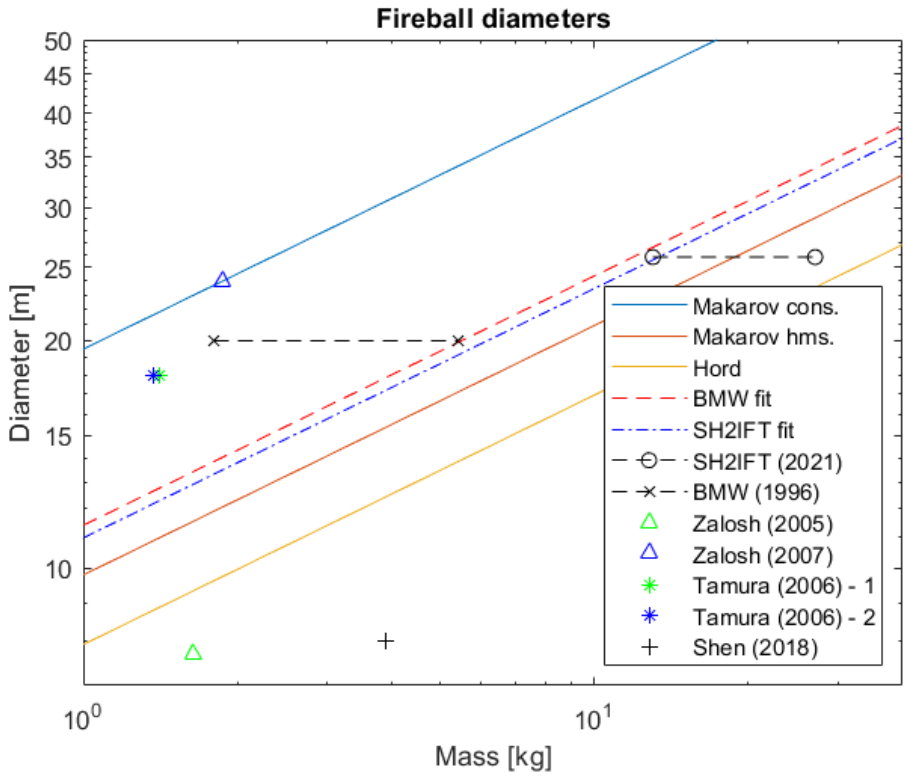

Figure 5.12: Diameter: fitting models vs experimental data.

Against this background, the new models proposed within this thesis were applied to investigate their suitability in the prediction of the experimental results. These correlations were obtained in order to fit the data from the BLEVE tests. As shown in Figure 5.12, these new models provide a similar description of the fireball dimension. This might hint that the actual masses of those two experiments are near to the upper and lower limits, as suggested in Chapter 4, respectively for the BMW and the SH2IFT tests, since the diameters show a similar increasing trend. Still, the mass uncertainties of the two experiments affect the reliability of these correlations.

For this reason, another model was adopted: the *I.G. EoS fit*. The results obtained are presented in Figures 5.13 and 5.14. The *I.G. EoS fit* overestimates all the experimental data, but the three whose shapes were flattened (Zalosh (2007) and the two from Tamura (2006)). This new correlation might be a good compromise between the

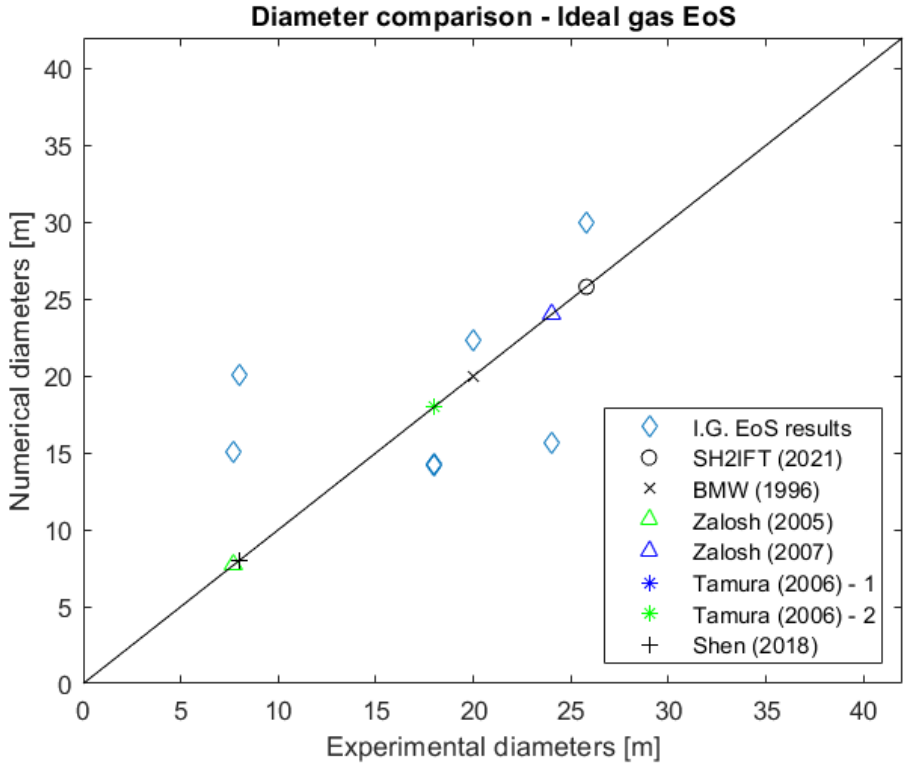

Figure 5.13: Numerical vs experimental diameters with the I.G. EoS fit model.

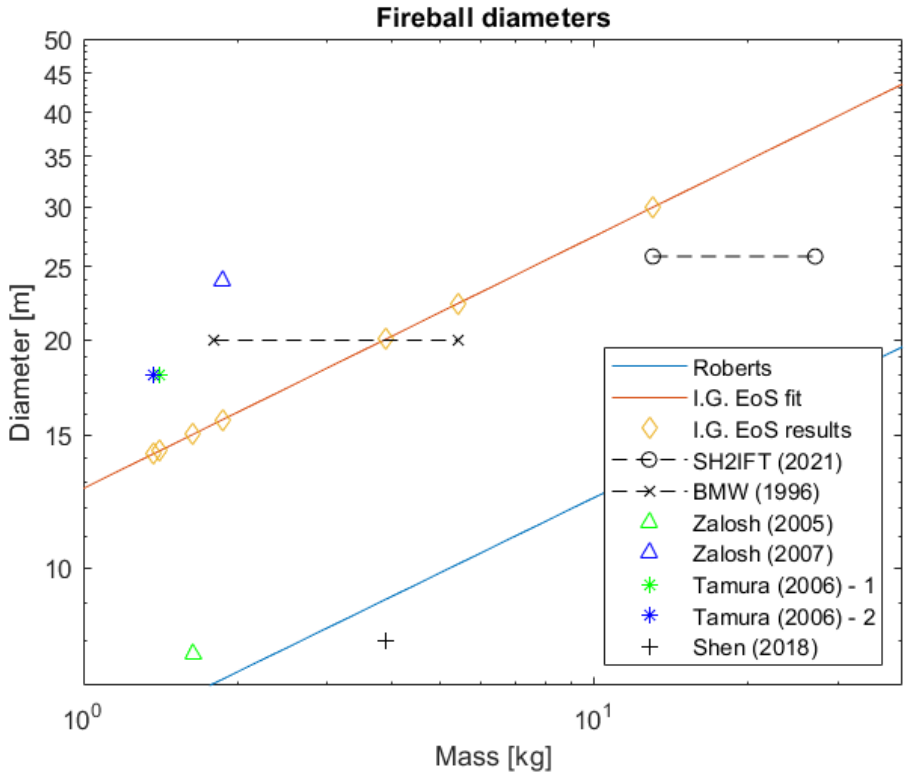

Figure 5.14: Diameter: I.G. EoS fit model vs experimental data.

literature models, which tend to underestimate the experimental data, and the most conservative one, that might cause an overestimation of the fireball dimensions in the majority of the cases.

To support the observations made until now, also the relative errors between the experimental data and the diameters calculated with all the models are presented in Table 5.3. The errors are reported in percentage and represent the relative distances of the models from the empirical data. Hence, a negative percentage means that the model underestimates the data, while a positive one implies it overestimates the experiment.

Table 5.3: Diameter relative errors.

	Roberts	**Hord**	**Makarov hms.**	**Makarov cons.**	**BMW fit**	**SH2IFT fit**	**I.G. EoS fit**
BMW (1.8kg)	-64.72%	-51.77%	-40.39%	18.60%	-30.66%	-33.28%	-22.51%
BMW (5.4kg)	-49.12%	-30.44%	-14.03%	71.06%	0.00%	-3.77%	11.76%
SH2IFT (13kg)	-47.14%	-27.73%	-10.69%	77.72%	3.90%	-0.02%	16.11%
SH2IFT (27kg)	-32.56%	-7.79%	13.95%	126.74%	32.56%	27.56%	48.14%
Zalosh (2005)	-11.17%	21.45%	50.09%	198.65%	74.59%	68.01%	95.12%
Zalosh (2007)	-70.23%	-59.29%	9.69%	0.10%	-41.48%	-43.69%	-34.60%
Tamura 1 (2006)	-63.90%	-50.65%	-39.01%	21.36%	-29.05%	-31.72%	-20.71%
Tamura 2 (2006)	-64.21%	-51.07%	-39.53%	20.32%	-29.66%	-32.32%	-21.39%
Shen (2018)	14.12%	56.03%	92.82%	283.68%	124.30%	115.84%	150.67%
Average error	46.35%	39.58%	38.91%	90.91%	40.69%	39.58%	46.78%
Average error 2	50.96%	40.10%	33.84%	64.87%	29.78%	29.92%	33.28%

The table points out the scatter of the data. Indeed, the errors show relevant variations between different experiments, regardless of the model considered. That highlights how none of the empirical correlations presented is able to describe all the hydrogen fireball diameters from the experiments properly. This is due to the fact that the fireball combustion process is a very complex phenomenon and, thus, the fireball can behave in a lot of different ways, depending on the conditions the test is performed.

For example, in Zalosh (2007) the PVB produced a large fireball from a small amount of fuel probably because the H_2 tank was placed under an SUV. This caused the fireball to be flattened after the vessel rupture and explosion.

Two different average errors are shown. The first one is calculated considering the absolute value of the errors of all the cases reported in Table 5.3, while the second one is obtained by neglecting the BMW (1.8kg), the SH2IFT (27kg) and the Shen (2018) data. This choice was made to try to reduce the comparison mistakes. Indeed, the average error values indicate that the best model is the *Makarov hms.*, with an average error of 38.91%, and that the Roberts and the *I.G. EoS fit* models have almost the same accuracy, with an inaccuracy of around 46%. However, this last observation does not take into account the results presented in Figures 5.11 and 5.14, where the Roberts equation underestimates most of the data. In addition, it is worth discussing the following considerations. In particular, the masses of the BLEVE tests are uncertain, but the values of 5.4kg and 13kg, respectively for the BMW and SH2IFT experiments, are considered to be more truthful data, given the explanations and considerations presented in Chapter 4. Also, the tank from Shen (2018) ruptured in a very atypical way, resulting in a small fireball even if the amount of fuel was bigger compared to the other PVB tests.

Without considering those three data, the *BMW fit* and the *SH2IFT fit* become the most accurate models, with an average error slightly under 30%. Also, the *Makarov hms.* and the *I.G. EoS fit* present lower average errors, that are around 33%.

Thanks to the considerations above, it can be inferred that the *I.G. EoS fit* seems to be the best model because it is quite conservative and, at the same time, it presents a lower average error, compared to the other models. However, this model cannot be validated since the number of data is limited and, then, other experiments are needed to be carried out.

5.2.2 Fireball duration

The analysis of fireball duration started with the models chosen from the literature: the momentum-driven and the buoyancy-driven formulas. Also, some fitting equations were adopted to better understand how the fireball duration changes with the mass, before proposing a more accurate model. Figure 5.15 shows the comparison with the experimental data.

The momentum-driven equation (the blue dashed line), which works for almost all the fuels with masses lower than 30,000kg, does not describe properly the hydrogen fireball duration, while the buoyancy-driven model (the red dashed line) seems to better characterize it. However, changing the equation coefficients to fit the data from the SH2IFT experiment, the *momentum-driven fit* (blue line) appears to be more accurate,

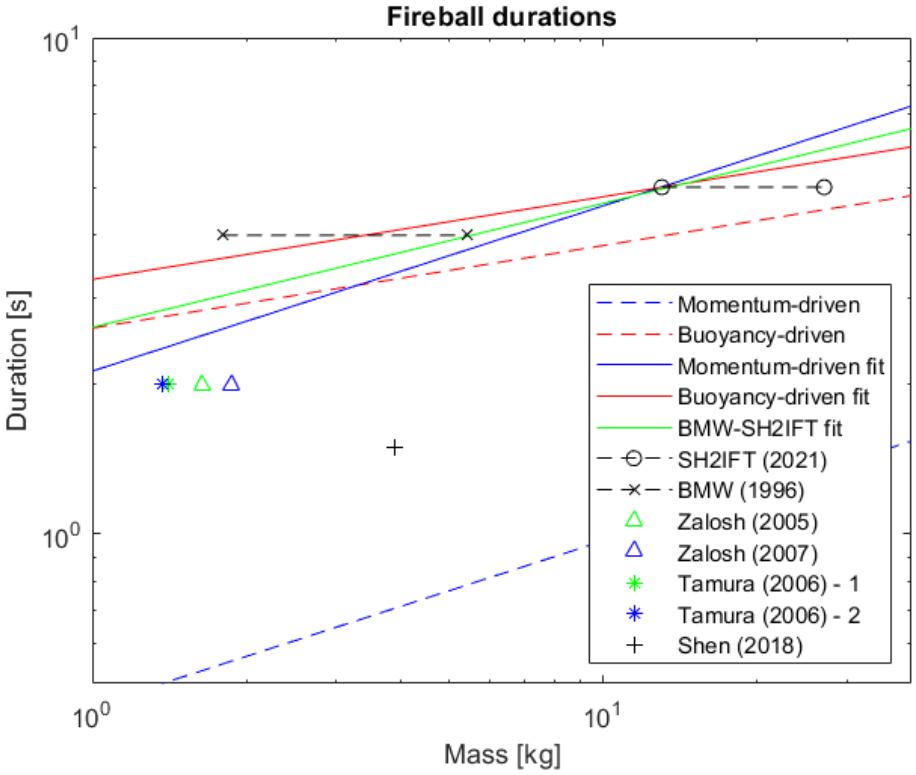

Figure 5.15: Duration: analytical models vs experimental data.

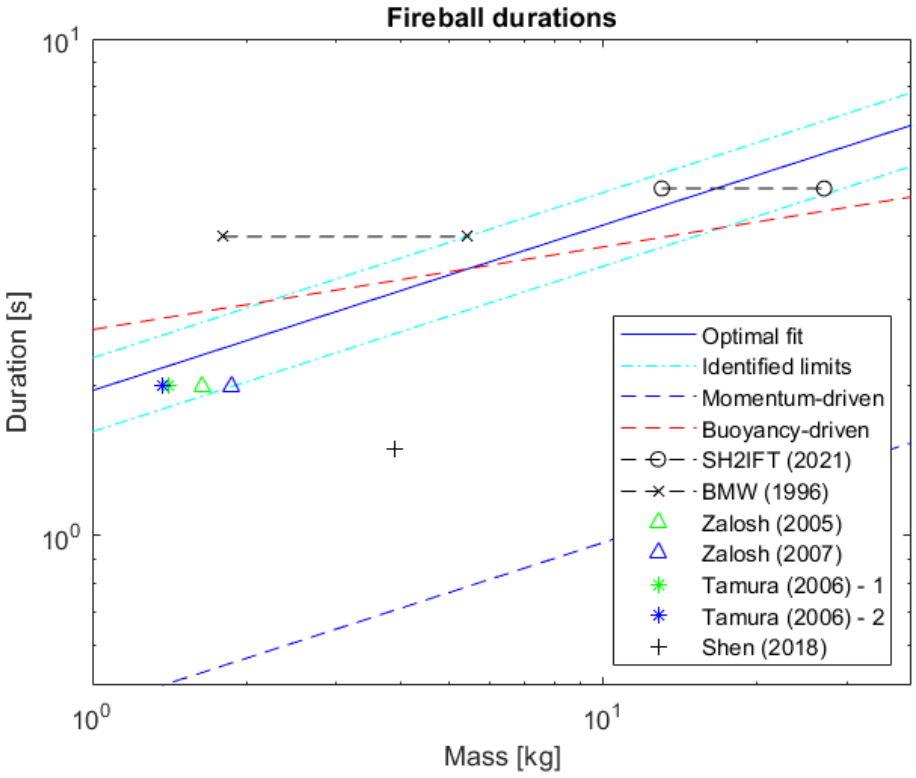

Figure 5.16: Duration: fitting models vs experimental data.

compared to the *buoyancy-driven fit* (red line).

Also the *BMW-SH2IFT fit*, obtained by changing both the coefficient and the exponent to fit the BMW and SH2IFT data, was implemented, but it cannot be considered reliable because of the uncertainties regarding the BLEVE tests masses.

Starting from these first observations, a new model, based on the momentum-driven description, has been proposed and the results can be observed in Figure 5.16. In addition to the blue line, which represents the new model, also two cyan dash-dotted lines are reported in the figure. Those lines indicate the equations that fit the highest and the lowest experimental data, without considering the Shen (2018) and the BMW tests in the case of 1.8kg of fuel. Thereby, almost all the experiments are included between those limits.

Differently from the dimensions, the fireball duration data are less scattered and this is visible from both Figures 5.15 and 5.16 and from Table 5.4, that show the relative errors related to the different models, in percentage.

Table 5.4: Duration relative errors.

	Momentum driven	**Buoyancy driven**	**Momentum driven fit**	**Buoyancy driven fit**	**BMW-SH2IFT fit**	**Optimal fit**
BMW (1.8kg)	-86.32%	-28.31%	-35.22%	-10.11%	-24.42%	-40.39%
BMW (5.4kg)	-80.26%	-13.90%	-6.58%	7.95%	-0.53%	-14.03%
SH2IFT (13kg)	-78.84%	-20.26%	0.17%	-0.02%	-0.88%	-7.83%
SH2IFT (27kg)	-73.00%	-9.93%	27.80%	12.93%	18.99%	17.60%
Zalosh (2005)	-73.47%	41.17%	25.59%	77.01%	47.68%	15.57%
Zalosh (2007)	-72.28%	44.29%	31.21%	80.92%	52.61%	20.74%
Tamura 1 (2006)	-74.79%	37.60%	19.31%	72.52%	42.10%	9.79%
Tamura 2 (2006)	-75.01%	37.00%	18.28%	71.78%	41.19%	8.84%
Shen (2018)	-52.78%	117.47%	123.52%	172.67%	144.52%	105.68%
Average error	74.08%	38.88%	31.96%	56.21%	41.44%	26.72%
Average error 2	75.78%	32.37%	16.86%	51.70%	30.83%	12.80%

Again, two different average errors were calculated, with the second one that does not consider the BMW (1.8kg), the SH2IFT (27kg), and the Shen (2018) data. In this case, the *average error 2* shows that the *optimal fit* describes quite well the fireball duration (neglecting the data just mentioned), with a relative error that does not exceed 20%, and is only 12.80% on average. Still, also this model cannot be validated because of the lack of a great amount of experimental data.

5.3 NASA tests

The experiments made by NASA in the 1960s give us a series of data related to the fireball diameters and durations. These data are studied separately from the ones referred to the PVB and BLEVE accidents, discussed in Section 5.2, because they involved tanks filled with a propellant, that was a mixture of LH_2 and LOX, and not only with hydrogen. In this case, only the mass of the fuel has been considered for the analysis and not the whole amount of fuel and oxidizer. For this reason, in the tests where the F:O ratio is different from 1:0, the masses reported in Table 3.2 have been reduced to take into account only the part of the fuel that was in the vessels.

5.3.1 Fireball dimension and duration

The experimental data related to the diameters and the durations of the fireballs have been fitted through the use of the MATLAB Curve Fitting Toolbox [53]. Thanks to this tool, it has been possible to find the best equations, listed below, that better describe the fireballs' behavior. Equation (5.1) is the diameter fitting equation:

$$D = 6.11 \cdot m_f^{1/3} \tag{5.1}$$

and Equation (5.2) is the momentum-driven fitting equation:

$$t = 0.45 \cdot m_f^{1/3} \tag{5.2}$$

This last relation concerns the fireball duration and was obtained neglecting the data with a mass of 7560kg, since it represents an isolated point and, thus, it was not considered reliable for the analysis. Figures 5.17 and 5.18 shows the results of the fitting.

As might be expected, the presence of LOX leads to different results in the fireball behavior. Indeed, the equations that better describe the fireball diameters and durations are very similar, if not identical, to the relations that can be found in literature, in particular to the Roberts equation (Equation (2.2)) and the Momentum-driven equation (Equation (4.22)).

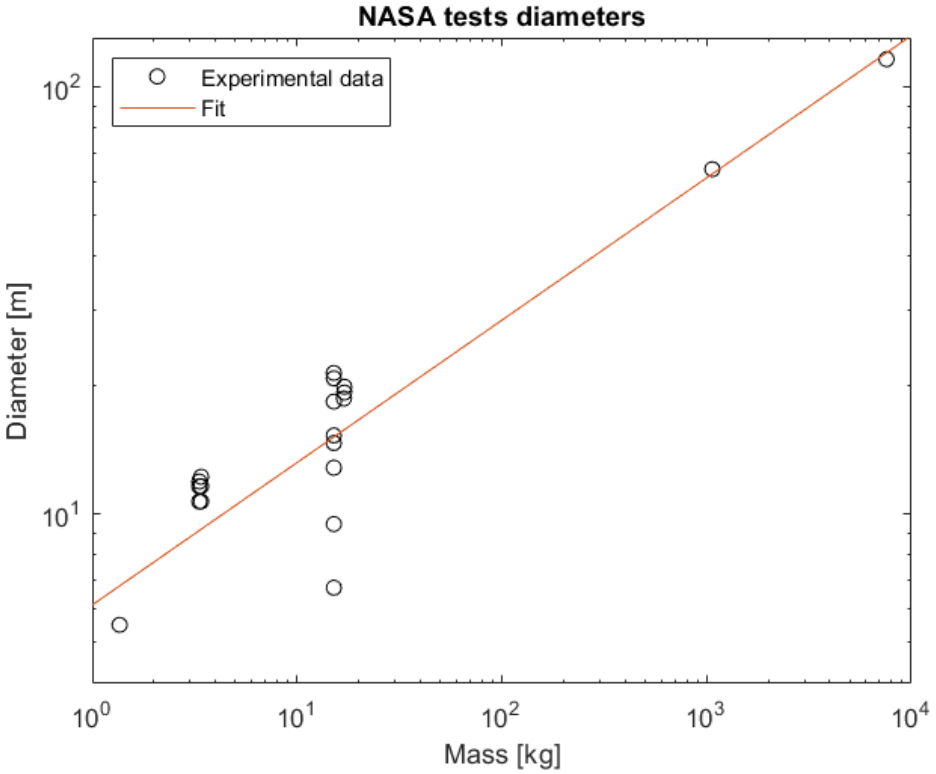

Figure 5.17: NASA tests diameter fitting.

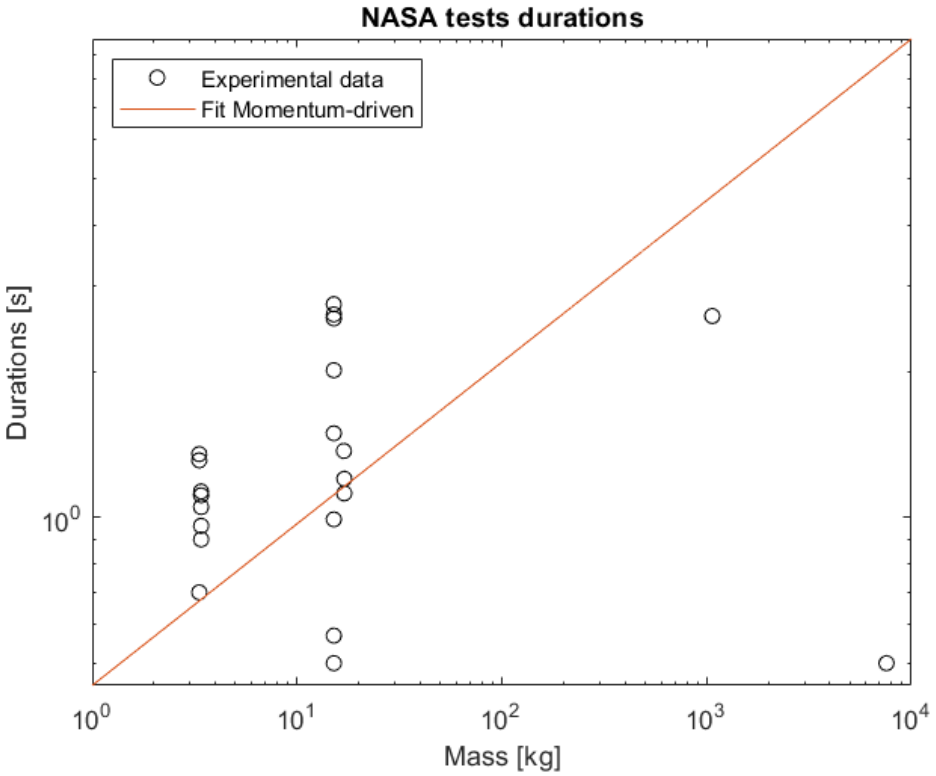

Figure 5.18: NASA tests duration fitting.

Comparing these results with the ones already analyzed, it seems that the presence of LOX reduces the fireball dimension and duration, when equal masses of fuel are considered. However, also for these tests the data are scattered, both those related to diameters and durations. Thus, it is difficult to find an equation that is able to describe all the experimental data.

6 Conclusions

In this thesis, the safety issues related to hydrogen storage systems were first analyzed. The tanks explosion events, both BLEVE and PVB, were presented and the main consequences have been described. In particular, the thermal hazard related to the fireball has been studied, many models present in literature and used to predict the fireball dimension and duration have been tested and new models have been proposed.

The analysis performed on the SH2IFT project fireball heat radiation showed that the combustion average temperature was around 1150K. Also, the fireball causes null or minor consequences when the target is not engulfed in the flames. However, the aftermaths become very severe when the target is located inside the fireball range, with a high probability of fatality. In addition, the fireball develops very quickly, giving no time to escape to any people involved, in the case such an event occurs. Moreover, also the damages caused by the pressure waves and the fragments, here not considered, have to be taken into account when a complete risk analysis of a BLEVE or PVB accident is performed.

A comparison of the experimental data, related to the hydrogen fireball generated from BLEVE and PVB, with the models selected from the literature has been carried out. It showed that the most used equations in safety engineering are not suitable for hydrogen fireballs, since they tend to underestimate the experimental data.

The new models, named *I.G. EoS fit* and *Optimal fit*, have been proposed, respectively for the fireball dimension and duration. They better describe the fireball behavior, even if the data, particularly the ones referred to the diameter, are scattered. In addition, the limited number of experiments performed until now regarding hydrogen fireballs does not allow to conduct a statistical analysis to understand the suitability and reliability of the proposed models.

Finally, also the NASA tests, related to LH_2/LOX propellant, were analyzed. From this data, it seems that the presence of LOX influences the fireball behavior, reducing both its dimension and duration when equal masses of fuel are considered.

Hydrogen is considered of key importance to fulfill the goals identified for the energy transition. The information provided by this study can be useful for the widespread employment of hydrogen technologies and, in particular, for a major understanding of the risks related to the use of this fuel.

The analytical models here presented are only one of several methods that can be used to predict fireball behavior. More detailed analyses might be carried out in future studies through numerical analyses by implementing different tools such as CFD or machine learning techniques.

A Heat Capacities at Constant Pressure of Chemical Compounds

Table A.1: Heat capacities for H_2, N_2, O_2, H_2O (adapted from [56]).

T (K)	**C_p (J/(mol · K))**			
	H_2	**N_2**	**O_2**	**H_2O**
0	0	0	0	0
300	28.849	29.125	29.388	33.596
500	29.254	29.582	31.092	35.225
700	29.444	30.754	32.990	37.449
900	29.873	32.090	34.361	39.998
1100	30.567	33.242	35.333	42.574
1300	31.421	34.147	36.006	45.065
1500	32.305	34.842	36.553	47.318
1700	33.144	35.377	37.057	49.292
1900	33.916	35.795	37.545	50.996
2100	34.618	36.127	38.020	52.458
2300	35.254	36.395	38.484	53.709
2500	35.832	36.615	38.933	54.777
2700	36.361	36.800	39.366	55.690
2900	36.848	36.957	39.780	56.474
3100	37.301	37.093	40.175	57.149
3300	37.728	37.213	40.549	57.736
3500	38.135	37.320	40.904	58.252
3700	38.525	37.417	41.239	58.712
3900	38.902	37.506	41.556	59.129
4100	39.269	37.589	41.854	59.514
4300	39.627	37.667	42.135	59.875
4500	39.975	37.743	42.400	60.221
4700	40.312	37.818	42.649	60.556
4900	40.637	37.893	42.884	60.883
5000	40.793	37.932	42.997	61.045

B Thermal effects with steady view factor

```
%Variables assignement
dSH=25.8;               %Fireball diameter [m]
rSH=dSH/2;              %Fireball radius [m]
tSH=5;                  %Fireball duration [s]
RH=0.662;               %Relative humidity
Tamb=18.5;              %Ambient temperature  [°C]
%Partial pressure of saturated vapor [Pa]
pw0=exp(23.18986-3816.42/(Tamb+273.15-46.13));
hSH=dSH;                %Fireball height [m] (assumed equal to max diameter)
X=rSH:1:200;            %Orizontal distance from fireball center [m]
L=(hSH^2+X.^2).^(0.5); %Distance from fireball center [m]
F=(rSH./L).^2;          %View factor (angle=0° to be conservative)
tauAir=2.02*(RH*pw0*(L-rSH)).^(-0.09);  %Atmospheric transmissivity

%Experimental Data

ExpDataTable=readtable('BLEVE02_heat_radiation1.csv', ...
    'PreserveVariableNames',true);
ExpDataMatrix=ExpDataTable{:,:};
qData=ExpDataMatrix(786937:789204,:);
qData(:,1)=qData(:,1)-3934.675;
dt=qData(2,1)-qData(1,1);

%% SEP avg Calculation

xexp=[50 70 90];                %Distances of bolometers [m]
Lexp=(hSH^2+xexp.^2).^(0.5);
Fexp=(rSH./Lexp).^2;
tauAirexp=2.02*(RH*pw0*(Lexp-rSH)).^(-0.09);
```

```
SEPexp=qData(:,2:4)./(tauAirexp.*Fexp)/1000; %[kW/m2]
SEPavg=mean(SEPexp(:,2:3),2);

%% Fitting 50m

%Start of instrument saturation
i=1;
while qData(i+1,2)>qData(i,2)
i=i+1;
end
startSat=i-2;

%End of instrument saturation
i=length(qData(:,2));
while qData(i-1,2)>qData(i,2) || qData(i-1,2)<2000
i=i-1;
end
endSat=i;

%Delta SEP at different distances (50m-70m ; 70m-90m)
DeltaSEP=zeros(length(qData(:,1)),2);
DeltaSEP(:,1)=SEPexp(:,1)-SEPexp(:,2);
DeltaSEP(:,2)=SEPexp(:,2)-SEPexp(:,3);
SEPfit=SEPexp(:,2)+DeltaSEP(:,2);

%Heat radiation at 50m with SEP avg [W/m2]
q50avg=SEPavg*tauAirexp(1)*Fexp(1)*1000;
%Heat radiation at 50m with SEP fit [W/m2]
q50fit=SEPfit*Fexp(1)*tauAirexp(1)*1000;

%% Thermal dose during time
thdose50avg=zeros(length(qData),1);
thdose50fit=zeros(length(qData),1);
thdose70=zeros(length(qData),1);
thdose90=zeros(length(qData),1);

td50avg=(q50avg(1)/1000)^(4/3)*dt;
td50fit=(q50fit(1)/1000)^(4/3)*dt;
td70=(qData(1,3)/1000)^(4/3)*dt;
td90=(qData(1,4)/1000)^(4/3)*dt;
thdose70(1)=td70;
```

```
thdose90(1)=td90;
for i=2:1:length(qData)
    td50avg=(q50avg(i)/1000)^(4/3)*dt;
    td50fit=(q50fit(i)/1000)^(4/3)*dt;
    td70=(qData(i,3)/1000)^(4/3)*dt;
    td90=(qData(i,4)/1000)^(4/3)*dt;
    thdose50avg(i)=thdose50avg(i-1)+td50avg;
    thdose50fit(i)=thdose50fit(i-1)+td50fit;
    thdose70(i)=thdose70(i-1)+td70;
    thdose90(i)=thdose90(i-1)+td90;
end

%% Thermal dose in space
%Analytical heat radiation [W/m2]
qAnalytic=max(SEPexp(:,2)).*tauAir.*F*1000;

%Analytical thermal dose [(kW/m2)^4/3*s]
tdAnalytic=(qAnalytic/1000).^(4/3)*tSH;
%Experimental thermal dose [(kW/m2)^4/3*s]
thdoseexp=[thdose50fit(end) thdose70(end) thdose90(end)];

%SEP to fit actual thermal dose data
SEPstar=(thdoseexp./tSH).^(3/4)./(Fexp.*tauAirexp);
SEPactualTD=mean(SEPstar);  %[kW/m2]

%Experimental thermal dose in space
qfit=SEPactualTD*tauAir.*F;  %[kW/m2]
tdfit=qfit.^(4/3)*tSH;
threshold1=80*ones(length(X));

%% Safety distance
thresholds=[80 240 1000 2000]; %Safety thresholds [(kW/m2)^4/3*s]
SDistances=zeros(length(thresholds),2);

for i=1:1:length(thresholds)
    k=1;
    while(tdAnalytic(k)>thresholds(i))
    k=k+1;
    end
    if k==1
        SDistances(i,1)=0;
```

```
    else
        SDistances(i,1)=X(k);
    end

    k=1;
    while(tdfit(k)>thresholds(i))
        k=k+1;
    end
    if k==1
        SDistances(i,2)=0;
    else
        SDistances(i,2)=X(k);
    end
end
```

C Thermal effects with dynamic view factor

```
%Experimental Data
ExpDataTable=readtable('BLEVE02_heat_radiation1.csv', ...
    'PreserveVariableNames',true);
ExpDataMatrix=ExpDataTable{:,:};
qData=ExpDataMatrix(786937:789204,:);
qData(:,1)=qData(:,1)-3934.675;
dt=qData(2,1)-qData(1,1);
totHeatDuration=dt*(length(qData(:,1))-1);  %Total heat radiation duration
startLiftOff=2/dt;                          %Element N of LiftOff starting
startLiftOff=ceil(startLiftOff);
endFireball=5/dt;                           %Element N of Fireball ending
endFireball=ceil(endFireball);
dSH=25.8;                                   %Fireball diameter [m]
rSH=dSH/2;                                  %Fireball radius [m]
tliftoff=2;                                 %Fireball liftoff time [s]
tSH=5;                                      %Fireball duration [s]
hmaxSH=dSH;                                 %Fireball maximum height [m]
htank=1;                                    %Height of hydrogen tank [m]
RH=0.662;                                   %Relative humidity
Tamb=18.5;                                  %Ambient temperature  [°C]
%Partial pressure of saturated vapor [Pa]
pw0=exp(23.18986-3816.42/(Tamb+273.15-46.13));
deltaX1=rSH-htank;  %Travelled space of fireball center before liftoff [m]
deltaX2=hmaxSH-rSH;  %Travelled space of fireball center after liftoff [m]
v1=deltaX1/tliftoff;                %Average velocity before liftoff [m/s]
v2=deltaX2/(tSH-tliftoff);           %Average velocity after liftoff [m/s]
dx1=v1*dt;                 %DeltaX per time-step of 5ms before liftoff [m]
dx2=v2*dt;                  %DeltaX per time-step of 5ms after liftoff [m]
hSH=zeros(length(qData(:,1)),1);     %Initialisation of height during time
hSH(1)=htank;
```

```
for i=2:1:startLiftOff
    hSH(i)=hSH(i-1)+dx1;
end
for i=startLiftOff+1:1:endFireball
    hSH(i)=hSH(i-1)+dx2;
end
for i=endFireball+1:1:length(hSH)
    hSH(i)=hmaxSH;
end

X=ceil(rSH):1:200; %Orizontal distance from fireball center [m]
L=zeros(length(hSH),length(X));
for i=1:1:length(hSH)
    for j=1:1:length(X)
        L(i,j)=(hSH(i)^2+X(j)^2)^(0.5); %Distance from fireball center [m]
    end
end
F=(rSH./L).^2; %View factor (angle=0° to be conservative)
tauAir=2.02*(RH*pw0*(L-rSH)).^(-0.09); %Atmospheric transmissivity
for i=1:1:length(hSH)
    for j=1:1:length(X)
        if tauAir(i,j)>1
            tauAir(i,j)=1;
        end
    end
end

%% SEP avg calculation

xexp=[50 70 90];                            %Bolometer distances [m]
Lexp=zeros(length(hSH),length(xexp));
for i=1:1:length(hSH)
    for j=1:1:length(xexp)
        Lexp(i,j)=(hSH(i)^2+xexp(j)^2)^(0.5);
    end
end
Fexp=(rSH./Lexp).^2;
tauAirexp=2.02*(RH*pw0*(Lexp-rSH)).^(-0.09);
SEPexp=qData(:,2:4)./(tauAirexp(:,1:3).*Fexp(:,1:3))/1000; %[kW/m2]
SEPavg=mean(SEPexp(:,2:3),2);
```

```
%% Fitting 50m

%Start of instrument saturation
i=1;
while qData(i+1,2)>qData(i,2)
i=i+1;
end
startSat=i-2;
%End of instrument saturation
i=length(qData(:,2));
while qData(i-1,2)>qData(i,2) || qData(i-1,2)<2000
i=i-1;
end
endSat=i;

%Delta SEP and radiation at different distances (50m-70m ; 70m-90m)
DeltaSEP=zeros(length(qData(:,1)),2);
DeltaSEP(:,1)=SEPexp(:,1)-SEPexp(:,2);
DeltaSEP(:,2)=SEPexp(:,2)-SEPexp(:,3);
SEPfit=SEPexp(:,2)+DeltaSEP(:,2);

%Heat radiation at 50m with SEP avg [W/m2]
q50avg=SEPavg.*tauAirexp(:,1).*Fexp(:,1)*1000;
%Heat radiation at 50m with SEP fit [W/m2]
q50fit=SEPfit*Fexp(1)*tauAirexp(1)*1000;

%% Thermal dose during time
thdose50avg=zeros(length(qData),1);
thdose50fit=zeros(length(qData),1);
thdose70=zeros(length(qData),1);
thdose90=zeros(length(qData),1);

td50avg=(q50avg(1)/1000)^(4/3)*dt;
td50fit=(q50fit(1)/1000)^(4/3)*dt;
td70=(qData(1,3)/1000)^(4/3)*dt;
td90=(qData(1,4)/1000)^(4/3)*dt;
thdose70(1)=td70;
thdose90(1)=td90;
for i=2:1:length(qData)
    td50avg=(q50avg(i)/1000)^(4/3)*dt;
    td50fit=(q50fit(i)/1000)^(4/3)*dt;
```

```
    td70=(qData(i,3)/1000)^(4/3)*dt;
    td90=(qData(i,4)/1000)^(4/3)*dt;
    thdose50avg(i)=thdose50avg(i-1)+td50avg;
    thdose50fit(i)=thdose50fit(i-1)+td50fit;
    thdose70(i)=thdose70(i-1)+td70;
    thdose90(i)=thdose90(i-1)+td90;
end

%% Thermal dose in space
%Analytic heat radiation [W/m2]
qAnalytic=max(SEPexp(:,2)).*tauAir(end,:).*F(end,:)*1000;
%Analytical thermal dose [(kW/m2)^4/3*s]
tdAnalytic=(qAnalytic/1000).^(4/3)*tSH;
%Experimental thermal dose [(kW/m2)^4/3*s]
thdoseexp=[thdose50fit(end) thdose70(end) thdose90(end)];

%SEP to fit actual thermal dose data
SEPstar=(thdoseexp./tSH).^(3/4)./(Fexp.*tauAirexp);
SEPactualTD=mean(max(SEPstar));  %[kW/m2]

%Experimental thermal dose in space
qfit=SEPactualTD.*tauAir(end,:).*F(end,:);  %[kW/m2]
tdfit=qfit.^(4/3)*tSH;
threshold1=80*ones(length(X),1);

%% Thermal dose function of space and time

SEPduringTime=SEPexp(:,2); %Average SEP (= SEP at 70m) during time (kW/m2)
qST=zeros(length(hSH),length(X));
thdoseST=zeros(length(hSH),length(X));

%Calculation of heat radiation during space and time
for i=1:1:length(hSH)
    for j=1:1:length(X)
        qST(i,j)=SEPduringTime(i)*tauAir(i,j)*F(i,j);
    end
end

%Calculation of thermal dose during space and time
tdST=(qST(1,:)).^(4/3)*dt;
thdoseST(1,:)=tdST;
```

```
for i=2:1:length(hSH)
    tdST=(qST(i,:)).^(4/3)*dt;
    thdoseST(i,:)=thdoseST(i-1,:)+tdST;
end

%% Safety distance
thresholds=[80 240 1000 2000]; %Safety thresholds [(kW/m2)^4/3*s]
SDistances=zeros(length(thresholds),2);

for i=1:1:length(thresholds)
    k=1;
    while(tdAnalytic(k)>thresholds(i))
    k=k+1;
    end
    if k==1
        SDistances(i,1)=0;
    else
        SDistances(i,1)=X(k);
    end

    k=1;
    while(tdfit(k)>thresholds(i))
        k=k+1;
    end
    if k==1
        SDistances(i,2)=0;
    else
        SDistances(i,2)=X(k);
    end
end
```

Bibliography

[1] United Nations Framework Convention on Climate Change. *What is the Kyoto Protocol?* URL: https://unfccc.int/kyoto_protocol.

[2] United Nations Framework Convention on Climate Change. *The Paris Agreement.* URL: https://unfccc.int/process-and-meetings/the-paris-agreement.

[3] International Energy Agency. "Net Zero by 2050: A Roadmap for the Global Energy Sector". In: *International Energy Agency* (2021), p. 224. URL: https://www.iea.org/reports/net-zero-by-2050.

[4] International Energy Agency. *The Future of Hydrogen.* Tech. rep. 2019. DOI: 10.1016/S1464-2859(12)70027-5. URL: https://www.iea.org/reports/the-future-of-hydrogen.

[5] R.D. McCarty, J. Hord, and H.M. Roder. *Selected Properties of Hydrogen (Engineering Design Data).* 1981.

[6] Hanane Dagdougui et al. "Chapter 7 - Hydrogen Logistics: Safety and Risks Issues". In: *Hydrogen Infrastructure for Energy Applications.* Ed. by Hanane Dagdougui et al. Academic Press, 2018, pp. 127–148. ISBN: 978-0-12-812036-1. DOI: https://doi.org/10.1016/B978-0-12-812036-1.00007-X. URL: https://www.sciencedirect.com/science/article/pii/B978012812036100007X.

[7] Federico Ustolin, Nicola Paltrinieri, and Filippo Berto. "Loss of integrity of hydrogen technologies: A critical review". In: *International Journal of Hydrogen Energy* 45.43 (2020), pp. 23809–23840. ISSN: 03603199. DOI: 10.1016/j.ijhydene.2020.06.021.

[8] Kees van Wingerden et al. "Medium-scale Tests to Investigate the Possibility and Effects of BLEVEs of Storage Vessels Containing Liquified Hydrogen". In: *Chemical Engineering Transactions* 90.December 2021 (2022), pp. 547–552. ISSN: 22839216. DOI: 10.3303/CET2290092.

[9] SINTEF. *SH2IFT - Safe Hydrogen Fuel Handling and Use for Efficient Implementation.* 2022. URL: https://www.sintef.no/projectweb/sh2ift/.

[10] *NIST. Nist Chemistry WebBook 2021.* URL: webbook.nist.gov/.

[11] Joakim Andersson and Stefan Grönkvist. "Large-scale storage of hydrogen". In: *International Journal of Hydrogen Energy* 44 (2019), pp. 11901–11919. DOI: 10.1016/j.ijhydene.2019.03.063.

[12] N.T. Stetson, S. McWhorter, and C.C. Ahn. *Introduction to hydrogen storage.* Vol. 2006. Elsevier Ltd., 2016, pp. 3–25. ISBN: 9781782423621. DOI: 10.1016/b978-1-78242-362-1.00001-8. URL: http://dx.doi.org/10.1016/B978-1-78242-362-1.00001-8.

[13] H. Barthelemy, M. Weber, and F. Barbier. "Hydrogen storage: Recent improvements and industrial perspectives". In: *International Journal of Hydrogen Energy* 42.11 (2017), pp. 7254–7262. ISSN: 03603199. DOI: 10.1016/j.ijhydene.2016.03.178. URL: http://dx.doi.org/10.1016/j.ijhydene.2016.03.178.

[14] G. Valenti. *Hydrogen liquefaction and liquid hydrogen storage.* Vol. 23. Elsevier Ltd., 2016, pp. 27–51. ISBN: 9781782423621. DOI: 10.1016/b978-1-78242-362-1.00002-x. URL: http://dx.doi.org/10.1016/B978-1-78242-362-1.00002-X.

[15] R.K. Ahluwalia, J.-K. Peng, and T.Q. Hua. *Cryo-compressed hydrogen storage.* Elsevier Ltd., 2016, pp. 119–145. ISBN: 9781782423621. DOI: 10.1016/b978-1-78242-362-1.00005-5. URL: http://dx.doi.org/10.1016/B978-1-78242-362-1.00005-5.

[16] Salvador M. Aceves et al. "High-density automotive hydrogen storage with cryogenic capable pressure vessels". In: *International Journal of Hydrogen Energy* 35.3 (2010), pp. 1219–1226. ISSN: 03603199. DOI: 10.1016/j.ijhydene.2009.11.069. URL: http://dx.doi.org/10.1016/j.ijhydene.2009.11.069.

[17] Alessandro Campari et al. "Applicability of Risk-based Inspection Methodology to Hydrogen Technologies: A Preliminary Review of the Existing Standards". In: *Proceedings of the 32nd European Safety and Reliability Conference (ESREL 2022)* August (2022). DOI: 10.3850/978-981-18-5183-4_R13-01-095-cd.

[18] F Ustolin et al. "Risk-based inspection planning for hydrogen technologies: review of currents standards and suggestions for modification". In: *IOP Conference Series: Materials Science and Engineering* 1193.1 (2021), p. 012075. ISSN: 1757-8981. DOI: 10.1088/1757-899X/1193/1/012075. URL: https://iopscience.iop.org/article/10.1088/1757-899X/1193/1/012075.

[19] Khlefa A. Esaklul. *Hydrogen damage.* Elsevier Ltd, 2017, pp. 315–340. ISBN: 9780081012192. DOI: 10.1016/B978-0-08-101105-8.00013-9. URL: http://dx.doi.org/10.1016/B978-0-08-101105-8.00013-9.

[20] Victoria Burt. *Corrosion in the Petrochemical Industry*. 2nd editio. ASM International, 2015.

[21] Hao Li et al. "Safety of hydrogen storage and transportation: An overview on mechanisms, techniques, and challenges". In: *Energy Reports* 8 (2022), pp. 6258–6269. ISSN: 23524847. DOI: 10.1016/j.egyr.2022.04.067. URL: https://doi.org/10.1016/j.egyr.2022.04.067.

[22] Nicola Paltrinieri, Knut Oien, and Valerio Cozzani. "Assessment and comparison of two early warning indicator methods in the perspective of prevention of atypical accident scenarios". In: *Reliability Engineering and System Safety* 108 (2012), pp. 21–31. ISSN: 09518320. DOI: 10.1016/j.ress.2012.06.017. URL: http://dx.doi.org/10.1016/j.ress.2012.06.017.

[23] G Hankinson and B J Lowesmith. *Integrated Design for Demonstration of Efficient Liquefaction of Hydrogen (IDEALHY) Fuel Cells and Hydrogen Joint Undertaking (FCH JU) Grant Agreement Number 278177 Title: Qualitative Risk Assessment of Hydrogen Liquefaction, Storage and Transportation*. Tech. rep. 278177. 2013.

[24] Tasneem Abbasi and S. A. Abbasi. "The boiling liquid expanding vapour explosion (BLEVE): Mechanism, consequence assessment, management". In: *Journal of Hazardous Materials* 141.3 (2007), pp. 489–519. ISSN: 03043894. DOI: 10.1016/j.jhazmat.2006.09.056.

[25] B. Hemmatian, E. Planas, and J. Casal. "On BLEVE definition, the significance of superheat limit temperature (Tsl) and LNG BLEVE's". In: *Journal of Loss Prevention in the Process Industries* 40.December 2015 (2016), p. 81. ISSN: 09504230. DOI: 10.1016/j.jlp.2015.12.001.

[26] Federico Ustolin. *Modelling of Accident Scenarios from Liquid Hydrogen Transport and Use*. 2021. ISBN: 978-82-326-6523-5. URL: https://hdl.handle.net/11250/2761199.

[27] A. M. Birk, C. Davison, and M. Cunningham. "Blast overpressures from medium scale BLEVE tests". In: *Journal of Loss Prevention in the Process Industries* 20.3 (2007), pp. 194–206. ISSN: 09504230. DOI: 10.1016/j.jlp.2007.03.001.

[28] SFPE. *Handbook of Fire Protection Engineering*. Ed. by Springer. 2016. ISBN: 9781493925643. URL: https://www.ptonline.com/articles/how-to-get-better-mfi-results.

[29] CCPS. *Guidelines for Vapor Cloud Explosion , Pressure Vessel Burst , BLEVE , and Flash Fire Hazards*. JOHN WILEY SONS & American Institute of Chemical Engineers, 2010. ISBN: 9780470251478.

[30] Robert C. Reid. "Possible Mechanism for Pressurized-Liquid Tank Explosions or BLEVE's". In: *Science* 203.4386 (1979), pp. 1263–1265. DOI: 10.1126/science.203.4386.1263. eprint: https://www.science.org/doi/pdf/10.1126/science.203.4386.1263. URL: https://www.science.org/doi/abs/10.1126/science.203.4386.1263.

[31] Joaquim Casal. *Evaluation of the effects and consequences of major accidents in industrial plants*. Elsevier, 2017.

[32] Federico Ustolin, Nicola Paltrinieri, and Gabriele Landucci. "An innovative and comprehensive approach for the consequence analysis of liquid hydrogen vessel explosions". In: *Journal of Loss Prevention in the Process Industries* 68.August (2020). ISSN: 09504230. DOI: 10.1016/j.jlp.2020.104323.

[33] J. M. Salla, M. Demichela, and J. Casal. "BLEVE: A new approach to the superheat limit temperature". In: *Journal of Loss Prevention in the Process Industries* 19.6 (2006), pp. 690–700. ISSN: 09504230. DOI: 10.1016/j.jlp.2006.04.004.

[34] Elham Abohamzeh et al. "Review of hydrogen safety during storage, transmission, and applications processes". In: *Journal of Loss Prevention in the Process Industries* 72.March (2021). ISSN: 09504230. DOI: 10.1016/j.jlp.2021.104569.

[35] Zhiyong Li et al. "Study on the harm effects of releases from liquid hydrogen tank by consequence modeling". In: *International Journal of Hydrogen Energy* 37.22 (2012), pp. 17624–17629. ISSN: 03603199. DOI: 10.1016/j.ijhydene.2012.05.141. URL: http://dx.doi.org/10.1016/j.ijhydene.2012.05.141.

[36] TNO (The Netherlands Organization of Applied Scientific Research). *CPR 14E Yellow Book – Methods for the Calculation of Physical Effects*. PSG2. The Hague, 2005, p. 870.

[37] Richard W. Prugh. "Quantitative evaluation of fireball hazards". In: *Process Safety Progress* 13.2 (1994), pp. 83–91. ISSN: 15475913. DOI: 10.1002/prs.680130211.

[38] Steven Betteridge and Lee Phillips. "Large scale pressurised LNG BLEVE experiments". In: *Institution of Chemical Engineers Symposium Series* 2015-January.160 (2015), pp. 1–12. ISSN: 03070492.

[39] A. F. Roberts. "Thermal radiation hazards from releases of LPG from pressurised storage". In: *Fire Safety Journal* 4.3 (1981), pp. 197–212. ISSN: 03797112. DOI: 10.1016/0379-7112(81)90018-7.

[40] W. E. Martinsen and J. D. Marx. "An improved model for the prediction of radiant heat from fireballs". In: *International Conference and Workshop on Modeling the Consequences of Accidental Releases of Hazardous Materials* (1999), pp. 605–621.

[41] Federico Ustolin and Nicola Paltrinieri. "Hydrogen fireball consequence analysis". In: *Chemical Engineering Transactions* 82 (2020), pp. 211–216. ISSN: 22839216. DOI: 10.3303/CET2082036.

[42] Eulàlia Planas and Joaquim Casal. "BLEVE-Fireball". In: *Handbook of Combustion Vol.1: Fundamentals and Safety* 1 (2015), pp. 1–26.

[43] K. Raj Phani. "A review of the criteria for people exposure to radiant heat flux from fires". In: *Journal of Hazardous Materials* 159.1 (2008), pp. 61–71. ISSN: 03043894. DOI: 10.1016/j.jhazmat.2007.09.120.

[44] P. J. Rew. *LD50 equivalent for the effect of thermal radiation on humans*. Tech. rep. 1997.

[45] S O'Sullivan and S Jagger. *Human Vulnerability to Thermal Radiation Offshore*. Tech. rep. 2004, p. 30.

[46] K. Pehr. "Aspects of safety and acceptance of LH2 tank systems in passenger cars". In: *International Journal of Hydrogen Energy* 21.5 (1996), pp. 387–395. ISSN: 03603199. DOI: 10.1016/0360-3199(95)00092-5.

[47] Robert Zalosh and Nathan Weyandt. "Hydrogen fuel tank fire exposure burst test". In: *SAE Technical Papers* (2005). ISSN: 26883627. DOI: 10.4271/2005-01-1886.

[48] Robert Zalosh. "Blast Waves and Fireballs Generated by Hydrogen Fuel Tank Rupture During Fire Exposure". In: *Fuel* April (2007), pp. 23–27.

[49] V. V. Molkov et al. "Dynamics of blast wave and fireball after hydrogen tank rupture in a fire in the open atmosphere". In: *International Journal of Hydrogen Energy* 46.5 (2021), pp. 4644–4665. ISSN: 03603199. DOI: 10.1016/j.ijhydene.2020.10.211.

[50] Chuanchuan Shen et al. "Consequence assessment of high-pressure hydrogen storage tank rupture during fire test". In: *Journal of Loss Prevention in the Process Industries* 55.March (2018), pp. 223–231. ISSN: 09504230. DOI: 10.1016/j.jlp.2018.06.016.

[51] Dmitriy Makarov et al. "Hydrogen Tank Rupture in Fire in the Open Atmosphere: Hazard Distance Defined by Fireball". In: *Hydrogen* 2.1 (2021), pp. 134–146. DOI: 10.3390/hydrogen2010008.

[52] George C. Marshall. *Size and duration of fireballs from propellant explosions*. Tech. rep. Huntsville, Alabama: NASA, 1965.

[53] MathWorks. *MATLAB*. URL: https://it.mathworks.com/products/matlab.html.

[54] Rino A. Michelin and Andrea Munari. *Fondamenti di chimica*. Third edition. Milan: Wolters Kluwer Italia, 2016.

[55] Ian H. Bell et al. "Pure and Pseudo-pure Fluid Thermophysical Property Evaluation and the Open-Source Thermophysical Property Library CoolProp". In: *Industrial & Engineering Chemistry Research* 53.6 (2014), pp. 2498–2508. DOI: 10.1021/ie4033999. eprint: http://pubs.acs.org/doi/pdf/10.1021/ie4033999. URL: http://pubs.acs.org/doi/abs/10.1021/ie4033999.

[56] Pasquale M. Sforza. *Theory of Aerospace Propulsion*. Elsevier, 2012, pp. 127–159. ISBN: 9781856179126. DOI: 10.1016/b978-1-85617-912-6.00004-9.

[57] Don W. Green and Robert H. Perry. *Perry's Chemical Engineers' Handbook*. 8th Editio. Vol. 4. 1. New York: McGraw-Hill, 2008. ISBN: 0071593136.

[58] Microsoft Corporation. *Microsoft Excel*. URL: https://www.microsoft.com/it-it/microsoft-365/excel.

[59] Kaveh Mazloomi and Chandima Gomes. "Hydrogen as an energy carrier: Prospects and challenges". In: *Renewable and Sustainable Energy Reviews* 16.5 (2012), pp. 3024–3033. ISSN: 13640321. DOI: 10.1016/j.rser.2012.02.028. URL: http://dx.doi.org/10.1016/j.rser.2012.02.028.